Intestine-enriched *apolipoprotein b* orthologs regulate stem cell differentiation and regeneration in planarians

Lily L. Wong [1,*], Christina G. Bruxvoort [1,2,*], Nicholas I. Cejda [1], Jannette Rodriguez Otero [3,4], and David J. Forsthoefel [1,5,#]

[1] Genes and Human Disease Research Program, Oklahoma Medical Research Foundation, Oklahoma City, Oklahoma

[2] Current address: Arthritis and Clinical Immunology Research Program, Oklahoma Medical Research Foundation, and Department of Pathology, University of Oklahoma Health Sciences Center, Oklahoma City, Oklahoma

[3] Howard Hughes Medical Institute, Department of Cell and Developmental Biology, University of Illinois at Urbana-Champaign, Urbana, Illinois

[4] Current address: Department of Education, Universidad Interamericana de Puerto Rico, Mercedita, Ponce, Puerto Rico

[5] Department of Cell Biology, University of Oklahoma Health Sciences Center, Oklahoma City, Oklahoma

* Authors contributed equally

[#] Correspondence:

David J. Forsthoefel, Ph.D.: david-forsthoefel@omrf.org

Abstract

Little is known about how lipid mobilization and utilization are modulated during stem-cell-driven tissue growth during regeneration. Planarian flatworms can regenerate all missing tissues in 10 days due to the proliferation and differentiation of pluripotent somatic stem cells called neoblasts. In planarians, diet-derived neutral lipids are stored in the intestine. Here, we identify two intestine-enriched paralogs of *apolipoprotein b, apob-1* and *apob-2,* that are required for regeneration. Consistent with apolipoproteins' known roles regulating neutral lipid (NL) transport in lipoprotein particles (LPs), NLs increased in the intestine upon simultaneous dsRNA-mediated knockdown of *apob-1* and *apob-2,* but were depleted in neoblasts and their progeny. *apob* knockdown reduced regeneration blastema morphogenesis, and delayed re-establishment of axial polarity and regeneration of multiple organs. Using flow cytometry, we found that neoblast progeny accumulated in *apob(RNAi)* animals, with minimal effects on neoblast maintenance or proliferation. In addition, ApoB reduction primarily dysregulated expression of transcripts enriched in neoblast progeny and mature cell types, compared to cycling neoblasts. Together, our results provide evidence that intestine-derived lipids serve as a source of metabolites required for neoblast differentiation. In addition, these findings demonstrate that planarians are a tractable model for elucidating specialized mechanisms by which lipid metabolism must be regulated during animal regeneration.

Introduction

Regeneration requires metabolites and energy for cell proliferation, differentiation, migration, and growth. Currently, specific mechanisms by which various metabolites are produced, transported, and utilized to drive regenerative growth are not well understood. In animals, neutral lipids (NLs) (e.g., triglycerides and cholesteryl esters) are stored in intracellular lipid droplets, which serve as central organelles for energy and lipid homeostasis (Walther et al., 2017; Olzmann and Carvalho, 2019). Lipid stores can be mobilized either by NL packaging and export in lipoprotein particles (LPs), or by lipolysis and secretion as FAs (Olofsson et al., 1999; Guo et al., 2009; D'Andrea, 2016). Mobilization enables transport to other tissues, for example between intestine, liver, and peripheral tissues such as brain and muscle in vertebrates, or between the fat body, intestine, nervous system, and imaginal discs in *Drosophila* (Lafontan and Langin, 2009; Heier and Kühnlein, 2018; Wong et al., 2019). Upon lipase-mediated hydrolysis, the fatty acids (FAs) and cholesterol produced serve as building blocks for membrane biosynthesis, substrates for energy via fatty acid beta oxidation, sources of acetyl-CoA and other precursors for histone modifications, and precursors of signaling molecules like eicosanoids and sphingolipids (Ruggles et al., 2013; Welte and Gould, 2017; Ly et al., 2020).

Considerable evidence indicates that dysregulation of NL and FA catabolism, biosynthesis, and transport can disrupt stem cell dynamics in adult somatic and germ line niches (Ito and Suda, 2014; Shyh-Chang and Ng, 2017; Clémot et al., 2020). For example, inhibiting fatty acid oxidation (FAO, the process of converting fatty acids to acetyl-CoA) causes symmetric production of differentiating progeny and stem cell depletion in the mammalian hematopoietic lineage (Ito et al., 2012). By contrast, in the adult mouse hippocampus, inhibiting FAO promotes exit from quiescence and proliferation of neural stem/progenitor cells (Knobloch et al., 2017). In *Drosophila*, compromising lipolysis and/or FAO causes intestinal stem cell necrosis (Singh et al., 2016), and loss of germ line stem cells (Sênos Demarco et al., 2019). On

70 the other hand, FAO-mediated production of acetyl-CoA (which, in addition to being a substrate
71 for energy production in the tricarboxylic acid cycle, is also a precursor for histone acetylation) is
72 required for differentiation, but not maintenance, of quiescent hematopoietic stem cells in
73 *Drosophila* larvae, illustrating the growing recognition of the intersection of lipid metabolism and
74 epigenetic regulation (Tiwari et al., 2020). Perturbing lipid synthesis and delivery also disrupts
75 stem cell dynamics. For example, inhibiting fatty acid synthase (required for *de novo*
76 lipogenesis) reduces proliferation by adult mouse neural stem and progenitor cells (Knobloch et
77 al., 2013). Similarly, mutations in *hydroxysteroid (17-beta) dehydrogenase 7*, a regulator of
78 cholesterol biosynthesis, cause premature differentiation of neural progenitors during
79 development (Driver et al., 2016). In culture, depriving human pluripotent stem cells of extrinsic
80 lipids promotes a "naive-to-primed" intermediate state, demonstrating the importance of
81 exogenous lipid availability for stem cell regulation (Cornacchia et al., 2019).
82 Because stem and progenitor cell activation, proliferation, and differentiation are central
83 to regeneration, these diverse observations underline the potential importance of lipid
84 metabolism during regenerative growth. Currently, however, evidence that lipid transport and
85 utilization influence regeneration is limited. In zebrafish, *leptin b* (a hormonal regulator of
86 systemic lipid metabolism) is one of the most upregulated genes during fin and heart
87 regeneration (Kang et al., 2016), and *apolipoprotein E* (a regulator of NL transport in LPs) is
88 upregulated during fin regeneration (Monnot et al., 1999). In the axolotl *Ambystoma mexicanum*,
89 genes involved in steroid, cholesterol, and fatty acid metabolism are among the most
90 upregulated at later stages of limb regeneration, when differentiation of cartilage and muscle
91 progenitors occurs (Voss et al., 2015). In a primary cell culture model of nerve injury, rat retinal
92 ganglion cells regrow projections after axotomy more efficiently in the presence of glial-derived
93 LPs, reinforcing the role of cholesterol in neuronal regeneration (Hayashi et al., 2004). In mice,
94 *low density lipoprotein receptor* deficiency delays liver regeneration and reduces hepatocyte
95 proliferation (Pauta et al., 2013). Similarly, elevated FA levels (induced by lipoprotein lipase

96 overexpression) causes lipotoxicity and compromises skeletal muscle regeneration
97 (Tamilarasan et al., 2012), while inhibition of peroxisomal FAO induces differentiation of
98 myogenic satellite cells and muscle hypertrophy during regeneration (Pala et al., 2018). During
99 skin wound repair, inhibiting triglyceride lipase-mediated lipolysis by dermal adipocytes
100 compromises recruitment of inflammatory macrophages and differentiation of extracellular-
101 matrix-secreting myofibroblasts (Shook et al., 2020).

102 Although these intriguing observations point to the importance of lipid trafficking and
103 metabolism, functional understanding of how lipid transport and metabolism impinges on stem
104 cell dynamics during regeneration is still quite limited, particularly in emerging animal models
105 with extensive regenerative capacity. In this study, we show that two *apolipoprotein b* orthologs
106 are required for NL transport, stem cell differentiation, and regeneration in the planarian
107 *Schmidtea mediterranea*, a freshwater flatworm capable of whole-body regeneration. In
108 planarians, pluripotent somatic stem cells called neoblasts divide and differentiate to replace
109 damaged and lost tissues after amputation (Newmark and Sánchez Alvarado, 2002; Reddien
110 and Sánchez Alvarado, 2004). As in *C. elegans* and *Drosophila*, diet-derived NLs are stored in
111 the planarian intestine in lipid droplets (Willier et al., 1925; Jennings, 1957; Mak, 2012; Heier
112 and Kühnlein, 2018). These lipid droplets have been proposed to be a source of metabolites
113 during extended fasting, as well as regeneration (Jennings, 1957; Gamo and Garcia-Corrales,
114 1987; Thommen et al., 2019), but whether delivery to neoblasts or their progeny is functionally
115 required for regeneration, has not been investigated. Previously, we demonstrated that
116 knockdown of an intestine-enriched transcription factor, *nkx2.2*, severely inhibited neoblast
117 proliferation and formation of the regeneration blastema, the unpigmented mass of tissue
118 produced after amputation (Forsthoefel et al., 2012). We now report that two intestine-enriched
119 *apolipoprotein b* orthologs were among the most down-regulated transcripts in *nkx2.2(RNAi)*
120 animals. In humans, ApoB protein mediates trafficking of NLs in LPs between the intestine, liver,
121 and target tissues, while in insects, ApoB function analogously to traffic NLs between the gut, fat

122 body, and other tissues (Olofsson et al., 1999; Palm and Rodenfels, 2020). In our study,
123 simultaneous knockdown of both planarian paralogs caused NL accumulation in the intestine,
124 NL depletion in neoblasts and their differentiation progeny, and delays in regeneration of
125 multiple cell types and organs. Flow cytometry analysis demonstrated that early neoblast
126 progeny accumulated in both uninjured and regenerating *apob(RNAi)* animals. This conclusion
127 was supported by transcriptomic analysis of *apob(RNAi)* animals, in which the gene expression
128 signature of differentiating progeny and mature cell types were disproportionately dysregulated
129 relative to that of neoblasts and progenitors. These results suggest a mechanism by which the
130 planarian intestine influences neoblast dynamics non-autonomously, and provide an entry point
131 into utilizing planarians as a model to understand regeneration-specific aspects of stem cell and
132 lipid metabolism.
133
134

135 # Results

136 **Planarian *apolipoprotein B* homologs are expressed by intestinal cells**

137 In order to identify transcripts dysregulated by inhibition of Nkx2.2, we used RNA
138 interference (RNAi) to knock down *nkx2.2,* and then extracted RNA for sequencing from control
139 and knockdown animals. 772 transcripts were downregulated and 710 transcripts were
140 upregulated (Fig. 1A-B and Table S1). These included many transcripts predicted to regulate
141 various aspects of lipid metabolism and small molecule transport (Table S2), consistent with a
142 role for Nkx2.2 in controlling expression of non-autonomous regulators. The majority (~2/3) of
143 downregulated transcripts and ~1/3 of upregulated transcripts were also normally enriched in
144 the intestines of uninjured animals (Fig. S1A-B). An ortholog of human *apolipoprotein b* ("*Smed-*
145 *apob-1*" or "*apob-1*") encoding conserved Vitellogenin, DUF1943, and von Willebrand Factor D
146 domains, was the second-most-downregulated transcript by significance and fold-change, while
147 a second paralog, *apob-2,* was also significantly downregulated (Fig. 1B-C, Fig. S1B-C, and
148 Table S1). Both transcripts were highly enriched in the intestine (Fig. 1C-D). Single cell
149 expression (Fincher et al., 2018) predicted that *apob-1* and *apob-2* were enriched in intestinal
150 phagocytes (absorptive cells responsible for digestion, nutrient storage, and metabolite
151 secretion) as well as late differentiating neoblast progeny, but not in neoblasts (Fig. S1D). We
152 confirmed these expression patterns using fluorescent in situ hybridization (FISH) (Fig. 1D and
153 Fig. S1E-F).

154

155 **ApoB paralogs are required for viability and regulate neutral lipid transport**

156 To determine whether ApoB orthologs might be required for homeostatic tissue renewal
157 and/or regeneration, we knocked down *apob-1* and *apob-2* using RNA interference (Rouhana et
158 al., 2013). In uninjured planarians, knockdown of either *apob-1* or *apob-2* individually had no
159 phenotype (not shown). However, after 3-5 double-stranded RNA (dsRNA) feedings, double

160 knockdown *apob(RNAi)* animals displayed a range of "mild" to "very severe" phenotypes, which
161 included head regression, ventral curling, and eventual lysis, phenotypes that are commonly
162 seen in planarians lacking functional neoblasts (Reddien et al., 2005a) (Fig. 2A). In addition, we
163 also observed that, prior to "very severe" phenotypes (Fig. 2A), animals gradually lost
164 pigmentation, suggesting a possible role for LPs in pigment biosynthesis, or generation/viability
165 of pigment cells. We also observed reduced motility (not shown), suggesting defects in ventral
166 epidermis, muscle, and/or neurons involved in light-responsiveness.

167 ApoB orthologs in vertebrates and insects regulate LP biogenesis and secretion
168 (Olofsson et al., 1999; Palm et al., 2012). To test whether ApoB protein was secreted, we made
169 a custom antibody recognizing the N-terminus of Smed-ApoB-1 (Fig. 2B-C). ApoB-1 protein was
170 enriched in the intestine, but also throughout the parenchyma, indicating that although *apob*
171 mRNAs are intestine-enriched, ApoB protein is robustly secreted and transported to peripheral
172 tissues (Fig. 2C). Expression was dramatically reduced in both regions in *apob-1;apob-2(RNAi),*
173 (*"apob(RNAi)"* hereafter for brevity) planarians, demonstrating that knockdown dramatically
174 reduced ApoB protein levels (Fig. 2C).

175 ApoB orthologs also regulate NL secretion and transport via LPs (Olofsson and Borén,
176 2005) (Palm and Rodenfels, 2020). To test whether planarian ApoB functioned similarly, we
177 knocked down both paralogs simultaneously, and evaluated NL distribution. In histological
178 sections, NLs (labeled with Oil Red O) were robustly elevated in both the intestine as well as
179 tissues surrounding the intestine, suggesting that both LP secretion by the intestine and
180 uptake/metabolism by peripheral tissues were compromised (Fig. 2D). Consistently, using thin
181 layer chromatography, we also found dramatic elevation of cholesteryl esters and triglycerides
182 in extracts from *apob(RNAi)* animals (Fig. 2E). These phenotypes predicted that delivery of NLs
183 to neoblasts and/or their progeny would be compromised by ApoB inhibition. To test this, we
184 dissociated control and RNAi planarians, and used an established flow cytometry protocol that
185 takes advantage of DNA labeling and sensitivity to X-irradiation to distinguish S/G2/M-phase

186 neoblasts ("X1"), G0/G1-phase neoblasts and their progeny ("X2"), and post-mitotic cells ("X-
187 ins," named for the fact that cells in this gate are insensitive to X-irradiation) (Hayashi et al.,
188 2006; Wagner et al., 2011) (Fig. 2F-H). In dissociated cells labeled with the NL probe BODIPY-
189 493/50, we found a dramatic reduction of fluorescence in both the X1 and X2 fractions in
190 *apob(RNAi)* animals vs. controls (Fig. 2I-J). Together, these data demonstrate that planarian
191 ApoB proteins are produced by the intestine and are likely secreted as LPs to transport NLs
192 from the intestine to stem cells and their progeny, thus playing an analogous role in NL
193 trafficking between the intestine, liver, and target tissues as in other animals.
194

195 ***apob* paralogs are required for polarity re-establishment and organogenesis during**
196 **regeneration**

197 To assess regeneration, we chose "mild" and "severe" uninjured animals after three
198 dsRNA feedings, amputated their heads, and assessed blastema morphogenesis, which
199 absolutely requires neoblast proliferation and differentiation (Reddien et al., 2005b; Scimone et
200 al., 2010; Zhu et al., 2015). Controls, *apob-1(RNAi)*-only, and *apob-2(RNAi)*-only regenerates
201 regenerated normally (Fig. 3A). However, *apob(RNAi)* double knockdown animals had reduced
202 posterior blastemas (head fragments) and anterior blastemas (trunk fragments) at 8 days post-
203 amputation (Fig. 3A). This phenotype was qualitatively more severe in fragments from "severe"
204 ("*apob-S"*) animals than "mild" ("*apob-M"*) animals (Fig. 3A). These results suggested that *apob-*
205 *1* and *apob-2* may function redundantly to regulate neoblasts.

206 Amputation induces changes in gene expression during planarian regeneration
207 (Wenemoser and Reddien, 2010; Wurtzel et al., 2015; Zeng et al., 2018). Using quantitative
208 PCR, we found that both *apob-1* and *apob-2* transcripts were upregulated in amputated tissue
209 fragments at two distinct time points during earlier stages of regeneration commonly associated
210 with neoblast proliferation (1-3 days) and differentiation (4-5 days) (Fig. S2A). This dynamic
211 expression pattern was recapitulated in RNA-Seq data from a 14-day time course of whole-body

212 planarian regeneration (Fig. S2B) (Zeng et al., 2018). Using quantitative capillary-based
213 Western blotting, we also found that ApoB-1 protein levels increased by 3-5 days after
214 amputation (Fig. S2C). In addition, accumulation of neutral lipids was sustained in 3- and 6-day
215 *apob(RNAi)* regenerates (Fig. S2D-E). Intriguingly, we also found that three planarian orthologs
216 of human lipoprotein receptors (which bind apolipoproteins, enabling LP uptake/metabolism)
217 were upregulated in regenerating brain and pharynx (Fig. S3A-D). These transcripts were
218 expressed in both *piwi-1*-mRNA-positive neoblasts as well as *piwi-1*-negative cells that were
219 likely to be differentiating neoblast progeny in the regenerating pharynx and blastema (Fig.
220 S3D). Two lipoprotein receptor genes (*ldlr-1* and *ldlr-2*) were also differentially expressed in the
221 whole-body regeneration RNA-Seq dataset (Fig. S3C) (Zeng et al., 2018). Using the Gene
222 Ontology, we identified additional planarian genes predicted to regulate lipid transport,
223 triglyceride, and cholesterol metabolism, and found that many of these transcripts were also up-
224 and down-regulated during regeneration (Fig S3E) (Table S3). Together, these observations
225 indicate that *apob-1, apob-2,* and other genes involved in neutral lipid metabolism are
226 differentially expressed in response to amputation, consistent with roles during regeneration.
227 The reduction of blastema size in *apob(RNAi)* fragments, the upregulation of *apob-1/-2*
228 during regeneration, and elevated neutral lipids in *apob(RNAi)* regenerates all suggested that
229 regeneration of specific cell types and organs would be affected by *apob* knockdown. To
230 investigate this, we amputated both "mild" and "severe" *apob(RNAi)* animals (Fig. 2A), and used
231 fluorescent whole-mount in situ hybridization (FISH) to further characterize *apob(RNAi)*
232 phenotypes. First, we asked whether an early event during regeneration, the differentiation of
233 anterior and posterior cells responsible for expressing cues required to re-establish axial
234 polarity, was affected (Reddien, 2018). Indeed, at three days post-amputation (3 dpa), the
235 number of both posterior *wnt11-2*-expressing cells (Fig. 3B) (Adell et al., 2009) and anterior
236 *notum*-expressing cells (Fig. 3C) (Petersen and Reddien, 2011) was reduced in *apob-M* and
237 *apob-S* fragments. By 6 dpa, although most *apob(RNAi)* fragments had regenerated more of

238 these cells, many fragments (especially *apob-S*) still had fewer than 5+ cells observed in all
239 control fragments (Figs. 3B-C). These data suggest that *apob* inhibition delays, but does not
240 completely abolish, regeneration of these cells.

241 Next, we asked whether *apob* RNAi affected regeneration of planarian organs including
242 the brain, pharynx, and intestine. Similar to polarity-cue-expressing cells, we observed that brain
243 and pharynx regenerated, but that these organs were smaller than in controls (Fig. S2F-G).
244 Quantitatively, at 6 dpa, both brain and pharynx were smaller in size, especially in *apob-S*
245 fragments (Fig. 3D-E). To assess intestine, we analyzed both head and tail regenerates, in
246 which a combination of neoblast-driven new cell production and remodeling of differentiated
247 tissue is required for successful regeneration (Forsthoefel et al., 2011). Newly regenerated
248 posterior branches were significantly shorter in *apob(RNAi)* head fragments (Fig. 3F). By
249 contrast, in tail fragments, length of the new anterior branch was not significantly affected (Fig.
250 3G). However, intestinal branches failed to fuse at the anterior midline, leading to a "split"
251 anterior branch phenotype in ~50% of *apob(RNAi)* tail fragments (Fig. 3G). Together, these
252 results suggest that ApoB reduction delays regeneration of multiple cell types and organs, and,
253 in the case of the intestine, might affect both differentiation as well as collective cell migration or
254 other processes required for remodeling.

255

256 ***apob* knockdown causes accumulation of early neoblast progeny**

257 Because *apob* knockdown disrupted multiple neoblast-driven processes during
258 regeneration, we asked whether defects in neoblast maintenance or proliferation were
259 responsible for the effects of *apob* RNAi on regeneration. First, we assessed neoblast numbers
260 using riboprobes that label all neoblasts (*piwi-1)*, or a subpopulation of putatively totipotent
261 neoblasts (*tgs-1*) (Reddien et al., 2005b; Zeng et al., 2018). In both uninjured planarians and
262 7.5-day regenerates, neoblast numbers and distribution were grossly normal (Fig. S4A-B). We
263 also assessed proliferation using anti-phospho-Histone H3 (Ser10) ("PS10") immunolabeling,

264 which marks cells in late G2 and M phase of the cell cycle (Hendzel et al., 1997; Newmark and
265 Sánchez Alvarado, 2000). In uninjured animals and 2-day head regenerates, the number of
266 mitotic neoblasts increased modestly in *apob-M,* but not *apob-S* samples (Fig. 4A-B). In 2-day
267 trunk regenerates, there was a more significant (~50%) increase in *apob-M* fragments, and a
268 modest increase in *apob-S* fragments (Fig. 4B). Together, these results suggested that ApoB
269 reduction might cause moderate hyperproliferation, or, alternatively, a modest mitotic delay,
270 without dramatically affecting *piwi-1+* or *tgs-1+* neoblast numbers. These mild phenotypes also
271 raised the possibility that ApoB reduction might preferentially dysregulate differentiation, rather
272 than proliferation or maintenance of actively cycling neoblasts.

273 We tested these possibilities quantitatively using flow cytometry. We dissociated
274 uninjured and regenerating planarians, and evaluated the proportions of cells in the "X1"
275 (S/G2/M neoblasts) and "X2" (G0/G1 neoblasts, early differentiating progeny, and X-insensitive
276 post-mitotic progeny) fractions (Fig. 4C-E) (Hayashi et al., 2006; Wagner et al., 2011). In
277 uninjured planarians, as well as 2-day and 7-day regeneration fragments, X1 neoblast numbers
278 were unaffected by *apob* knockdown (Fig. 4E), consistent with the moderate effect of *apob*
279 RNAi on neoblast proliferation (Fig. 4A-B). By contrast, in uninjured planarians as well as 2-day
280 trunk fragments, the proportion of cells in the X2 gate increased significantly by ~30-40% (Fig.
281 4E) in *apob(RNAi)* animals vs. control. In 2 dpa head fragments, there was also a modest, but
282 statistically insignificant increase (~15%) in the X2 fraction (Fig. 4E). Because the X2 fraction
283 includes both cycling G1-phase neoblasts and differentiating post-mitotic progeny (Eisenhoffer
284 et al., 2008; Hayashi et al., 2010), these results suggested that *apob* inhibition might cause
285 lengthening of G1 phase of the cell cycle, and/or a delay in differentiation of early neoblast
286 progeny, either of which could increase the proportion of cells in X2.

287 In order to distinguish between these possibilities, we examined the X2 fraction in
288 uninjured planarians 24 hr after X-irradiation, which preferentially ablates over 95% radiation-
289 sensitive cycling neoblasts in both X1 and X2, without affecting the majority of early neoblast

290 progeny in X2 (Eisenhoffer et al., 2008; Zeng et al., 2018). As expected, the X1 fraction (again,
291 comprised of S/G2/M-phase neoblasts) was almost completely eliminated in both control and
292 *apob(RNAi)* samples (Fig. 4F-G). However, although irradiation reduced the proportion of X2
293 cells by ~48-56% in both control and *apob(RNAi)* animals (Fig. 4G), the expansion of the X2
294 fraction persisted in *apob-M* (~62.5% increase) and *apob-S* animals (~42.5% increase) relative
295 to controls (Fig. 4G). This increase in radiation-insensitive cells in X2 strongly suggested that
296 the primary defect in *apob* knockdown animals was a delay in early differentiation of neoblast
297 progeny.

298 Intriguingly, the increase in radiation-resistant X2 cells was transient: by 48 hr post-
299 irradiation, the proportions of X2 cells in *apob(RNAi)* samples were only modestly (and not
300 significantly) elevated (Fig. 4G). Similarly, the increase in the X2 fraction was more modest in 7-
301 day trunk regenerates (17-26%), and was not observed in head fragments (Fig. S4C). These
302 observations suggest that differentiation is delayed, but not arrested, in *apob(RNAi)* animals.
303 That is, at later time points, progeny have differentiated further, and now reside in the "X-ins"
304 gate with more mature progeny and post-mitotic cell types. Alternatively, some early progeny
305 might undergo apoptosis or necrosis at later time points, reducing the apparent accumulation of
306 neoblast progeny in X2. This scenario is consistent with the death phenotype observed in very
307 severe knockdown animals, which exhibit ventral curling and head regression, similar to animals
308 in which neoblast numbers or function is reduced (Fig. 2A) (Reddien et al., 2005a). Either
309 possibility could explain why regeneration proceeds in *apob(RNAi)* animals, but at a reduced
310 rate (Fig. S2F-G). Additional investigation will be required to discern the ultimate fate of early
311 progeny level at the single cell level.
312

313 **ApoB reduction preferentially dysregulates expression of transcripts enriched in**
314 **differentiating neoblast progeny and mature cell types**

315 Our flow cytometry data suggested that the major defect in uninjured and regenerating
316 *apob(RNAi*) animals was a delay in the differentiation of neoblast progeny. To test this
317 interpretation further, we used global (whole animal) transcriptomic analysis to assess gene
318 expression in *apob(RNAi)* animals. We predicted that if ApoB is required by cycling neoblasts,
319 then *apob* knockdown would preferentially dysregulate known neoblast-enriched transcripts,
320 and transcripts involved in cell cycle progression, DNA replication, etc. Conversely, if ApoB is
321 primarily required by differentiating progeny, then we would predict altered expression of
322 transcripts known to be enriched in neoblast progeny, and with functional roles in differentiation
323 and maturation. To test these predictions, we used RNA-Seq to identify transcripts that were
324 differentially expressed (DE) in *apob-M* (842 upregulated and 1139 downregulated transcripts)
325 and *apob-S* animals (1960 upregulated and 2547 downregulated transcripts), relative to control
326 (Table S4A-D). Then, we used the Gene Ontology (GO) to identify patterns of dysregulation in
327 specific functional categories. In addition, we cross-referenced the global *apob* "dysregulation
328 signature" with recently published bulk transcriptomes of flow-sorted neoblasts (Zeng et al.,
329 2018), as well as single cell transcriptomes from whole planarians representing all planarian cell
330 types and states, from cycling neoblasts to mature post-mitotic progeny (Fincher et al., 2018).
331 For upregulated transcripts, "lipid metabolism" was the fifth-most over-represented
332 Biological Process (BP) term in *apob-M* animals, and was the most over-represented category
333 in *apob-S* animals (Fig. 5A, Table S5A-B). Enrichment of the subcategories of acylglycerol, fatty
334 acid, steroid, and glycerolipid metabolism was consistent with known roles of ApoB orthologs,
335 and suggested a possible compensatory gene expression response to *apob(RNAi)*-induced NL
336 transport disruption. *apob* knockdown also more broadly upregulated carboxylic acid
337 metabolism, which includes fatty acids but also amino acids and tricarboxylic acid cycle
338 intermediates (Fig. 5A, Table S5A-B). Interestingly, transcripts whose orthologs coordinate
339 morphogenesis of multiple tissues including epidermis, nervous system, and the eye were also
340 upregulated. Of note, transcripts predicted to regulate "differentiation" or "specification," but not

341 "proliferation," were common in these categories. *apob(RNAi)* also downregulated transcripts in
342 additional metabolism categories, including gluconeogenesis, glycolysis, pyruvate, and
343 nucleotide metabolism (e.g., NADH and ADP), as well as ion transport, indicating wide-ranging
344 dysregulation of metabolite processing and trafficking, especially in *apob-S* animals (Fig. 5B,
345 Table S5C-D). Downregulated transcripts also included numerous putative regulators of cilium
346 morphogenesis and function (possibly reflecting disruption of ciliated epidermal and/or
347 protonephridial cell function or numbers), muscle morphogenesis and function (consistent with
348 motility defects in *apob(RNAi)* animals), and extracellular matrix organization and collagen
349 metabolism (Fig. 5B, Table S5C-D). Again, categories related to the cell cycle, mitosis, etc.
350 were not enriched among downregulated transcripts. Together, these data suggest that ApoB
351 reduction mainly affects metabolism, cell/tissue differentiation, and functions of mature cell
352 types, but not processes required specifically for cellular proliferation.

353 To test whether *apob* preferentially dysregulated gene expression during differentiation,
354 we cross referenced our DE transcript list with recently published bulk transcriptomes from flow-
355 sorted X1, X2, and Xins cell fractions (above), as well as cells sorted based on their expression
356 of PIWI-1 protein, a widely used marker whose expression is thought to mark lineage "states" in
357 planarians (e.g., high PIWI-1 levels in neoblasts, low PIWI-1 levels in some neoblasts and all
358 differentiating progeny, and negligible PIWI-1 levels in mature post-mitotic cells) (Fig. 5C-D and
359 Fig. S5A-D) (Zeng et al., 2018). We first identified transcripts that were most highly enriched
360 (e.g., 2-fold vs. other fractions, see Methods) to generate a "signature" transcript list for each
361 fraction or state (Fig. S5A-D). We then asked what percent of these signature transcripts were
362 dysregulated in *apob-M* and *apob-S* animals. *apob* RNAi dysregulated signature transcripts in
363 all three categories (Fig. 5C-D, Fig. S5A-D). However, compared to X1 or "PIWI-HI" signature
364 transcripts, 2-4 times as many transcripts were up- or down-regulated in X2 and "PIWI-LO" cell
365 classes, which are thought to include both neoblasts and early progeny (Fig. 5C-D) (Eisenhoffer
366 et al., 2008; Zeng et al., 2018). More X2 and PIWI-LO signature transcripts, as a percentage,

367 were also up- or down-regulated relative to signature transcripts of mature cell types in Xins and
368 PIWI-NEG fractions (Fig. 5C-D).

369 Using a similar approach, we also compared the gene expression signature of
370 *apob(RNAi)* animals with single cell transcriptomes to determine how *apob* RNAi affected
371 expression of genes thought to mark specific cell states during the progression from pluripotent
372 neoblast to mature cell types in eight planarian lineages (Fincher et al., 2018). Strikingly, in
373 *apob(RNAi)* animals, in three well characterized lineages (epidermis, intestine, and
374 protonephridia), the percentage of dysregulated "state-enriched" transcripts was lowest for
375 subclusters likely to be neoblast/progenitor subpopulations or early transition states ("N/TS"),
376 but higher for later progeny ("P") and mature cell types ("M") (Fig. 5E-G). These trends were
377 also observed in less well-characterized lineages such as muscle, pharynx, and *cathepsin*-
378 positive cells (Fig. S6A-F), in which *apob* RNAi dysregulated the smallest proportions of genes
379 in subclusters with the highest *piwi-1* mRNA levels, while preferentially dysregulating transcripts
380 enriched in later progeny and mature cell types (Fig. S6A-F).

381 Together, the results of these transcriptome comparisons are strikingly parallel to
382 analyses of *apob(RNAi)* phenotypes *in vivo* and as assessed by flow cytometry. Altogether, the
383 most straightforward interpretation of our data is that the effect of ApoB reduction on
384 regeneration is not due to disrupted neoblast maintenance or proliferation, but rather, to a delay
385 in the differentiation and maturation of neoblast progeny, which could be caused or exacerbated
386 by disrupted functions of mature cell types.

387

388

389 ## Discussion

390 We demonstrate that reducing ApoB levels blocks NL export from the intestine and
391 uptake by neoblasts and their progeny. This deprives neoblasts and their post-mitotic daughters
392 of LP cargo needed for efficient differentiation and maturation, and may also compromise the
393 function(s) of mature tissues including the intestine, muscle, nervous system, and epidermis --
394 both of which could slow regeneration. Because *apob-1* and *apob-2* are downregulated by
395 inhibition of *nkx2.2,* an intestine-enriched transcription factor also required for regeneration
396 (Forsthoefel et al., 2012), our results provide a specific example of how the planarian intestine
397 can non-autonomously influence neoblast dynamics, and also suggest an understudied role for
398 Nkx-family transcription factors in regulation of lipid metabolism. Intriguingly, unlike *nkx2.2*
399 RNAi, *apob* knockdown does not reduce the abundance of phosphoHistone-H3-S10-positive
400 neoblasts, indicating that the proliferative defect in *nkx2.2(RNAi)* animals is not caused by *apob*
401 reduction, and additional downstream regulators of proliferation remain to be discovered.
402 Intriguingly, dozens of additional regulators of lipid metabolism and transport of other
403 metabolites are downregulated in *nkx2.2(RNAi)* animals, suggesting additional ways by which
404 the intestine could influence neoblasts and their niche. Our study complements other recent
405 efforts demonstrating that global triglyceride reduction, caused by inhibition of an exocyst
406 complex component, increases planarian neoblasts and inhibits regeneration (Deb et al., 2020),
407 and that inhibition of *nuclear hormone receptor-1 (nhr-1)* increases LD size and abundance,
408 while reducing acetyl-CoA and planarian reproductive organogenesis (Zhang et al., 2018).

409 *apob* knockdown could affect neoblast differentiation through multiple mechanisms.
410 First, a simple explanation is that depriving neoblasts and progeny of TGs and CEs impairs their
411 ability to produce energy through FAO, elaborate membranes and organelles during
412 differentiation into mature cell types, and/or produce signaling lipids such as sphingolipids or
413 eicosanoids. Second, our data also suggest that lipid accumulation in *apob(RNAi)* planarians

414 may induce cellular stress, inflammation, autophagy, and/or compromise the functions of other
415 tissues that signal to neoblasts, particularly muscle, thereby indirectly influencing stem cell
416 differentiation (Reddien, 2018). Third, LPs also transport fat soluble vitamins (Rigotti, 2007;
417 Hussain, 2014), as well as morphogens like Hedgehog and Wnt (Panáková et al., 2005).
418 However, ApoB deficiency delays differentiation of multiple planarian lineages (including cells
419 expressing polarity cues), and dramatically dysregulates lipid metabolism at both biochemical
420 and gene expression levels. This suggests that ApoB proteins' functions in lipid transport
421 underlie roles in stem cell dynamics. Nonetheless, further characterization of planarian LP cargo
422 may yield additional insights. Finally, in other animals, disruptions in FAO/lipid metabolism
423 cause deficiencies in acetyl-CoA production and histone acetylation, causing genome-wide
424 epigenetic dysregulation that can alter stem cell pluripotency and differentiation (Ly et al., 2020;
425 Tiwari et al., 2020).

426 More broadly, the effect of *apoB* knockdown on regeneration raises additional questions
427 and priorities. First, although the existence of LDs in planarian neoblasts has been known for
428 decades (Betchaku, 1967), the roles of this intriguing organelle have not been investigated. We
429 did not assess neoblast LDs specifically, but *apoB* knockdown dramatically reduced NL content
430 in both X1 (S/G2/M) and X2 (G0/G1) neoblast fractions, suggesting that ApoB and LPs could
431 influence neoblast LD content and/or function. Once thought of as static storage particles,
432 recent work has demonstrated that LDs in animal cells are dynamic, multi-functional organelles
433 that regulate nutrient sensing, cell stress responses, and even intracellular localization of
434 histones, transcription factors, and other proteins (Welte and Gould, 2017; Olzmann and
435 Carvalho, 2019). Additionally, although emerging data suggest LDs as a potential therapeutic
436 target in cancer stem cells (Tirinato et al., 2017; Cruz et al., 2020), our knowledge of the
437 regulation and functions of LDs in stem cells, especially during regeneration, is limited. Studies
438 in planarians and other regeneration models could further illuminate the roles of this organelle.
439 Second, coordinated metabolic shifts between glycolysis and oxidative phosphorylation may be

440 a widespread aspect of stem cell transitions between quiescence, proliferation, and
441 differentiation, and extrinsic lipids can influence these states (Ito and Suda, 2014; Shyh-Chang
442 and Ng, 2017; Clémot et al., 2020; Ly et al., 2020). Indeed, our RNA-Seq data suggest that
443 transcription of regulators of amino acid metabolism, glycolysis, the tricarboxylic acid cycle, and
444 other metabolic pathways respond to *apob(RNAi)*, suggesting that planarian stem cell
445 metabolism is just as dynamic as in other animals. The fact that *apob(RNAi)* seems to primarily
446 affect post-mitotic states also suggests that planarian neoblasts might rely primarily on
447 glycolysis for energy, and shift to lipid metabolism and oxidative phosphorylation during
448 differentiation, as in other systems (Shyh-Chang et al., 2013; Love et al., 2014; Sinclair et al.,
449 2020). Again, studies in animals with high regenerative capacity could generate greater insights
450 into whether and how injury can induce metabolic switching. Finally, we found that expression of
451 *apob-1* and *apob-2,* as well as numerous other regulators of NL metabolism were dynamically
452 up- and down-regulated at the transcript level during regeneration (Fig. S3E). This suggests that
453 coordination of lipid metabolism is part of a genome-encoded program of regenerative gene
454 expression. Unraveling which transcription factors, chromatin modifiers, and other regulators are
455 responsible for such regulation is thus a third priority for future study.
456 In summary, we have identified *apolipoprotein B* orthologs and neutral lipid metabolism
457 as important regulators of stem cell dynamics and regenerative tissue growth. Efforts to define
458 the precise functions of NLs and their metabolic derivatives in planarians and other models will
459 improve our understanding of metabolic requirements of stem-cell-driven regeneration. In
460 addition, because lipid metabolism is amenable to pharmacological manipulation (Gaudet et al.,
461 2017), these studies may provide new insights relevant to the dual goals of promoting repair of
462 damaged human tissues, and inhibiting growth in pathological contexts like cancer.
463
464
465

466 # Methods

467 **Ethics Statement**

468 Anti-ApoB-1 antibodies were generated by GenScript USA (Piscataway, NJ), an OLAW,
469 AAALAC, and PHS-approved vendor. GenScript's animal welfare protocols were approved by
470 OMRF IACUC. No other vertebrate organisms were used in this study.

471

472 **Planarian care**

473 Asexual *Schmidtea mediterranea* (clonal line CIW4, RRID:NCBITaxon:79327) (Sánchez
474 Alvarado et al., 2002) were maintained in 0.5 g/L Instant Ocean salts with 0.0167 g/L sodium
475 bicarbonate dissolved in Type I water (Roberts-Galbraith and Newmark, 2013), and fed with
476 beef liver paste. Planarians were starved 7-10 days prior to initiating RNAi. Animals were 2-5
477 mm in length for most experiments except flow cytometry, for which 5-10 mm animals were
478 used. Uninjured, intact animals were randomly selected from large (300-500 animal) pools.

479

480 **Cloning and expressed sequence tags**

481 Transcripts were cloned as previously described (Forsthoefel et al., 2020). Sequences
482 were identified in the dd_Smed_v6 transcriptome (Brandl et al., 2016) and the Smed_ESTs3
483 library (Zayas et al., 2005). These included *nkx2.2* (dd_2716_0_1/PL08007A2A07),
484 *apob-1* (dd_636_0_1/PL06004B2E09), *apob-2* (dd_194_0_1/PL08004B1B10), *ldlr-1*
485 (dd_9829_0_1), *ldlr-2* (dd_5596_0_1/PL04021A1C10), *vldlr-1* (dd_1510_0_1/PL05007B1H03),
486 *notum* (dd_24180_0_1), *wnt11-2* (dd_16209_0_1), *choline acetyltransferase/ChAT*
487 (dd_6208_0_1), *laminin* (dd_8356_0_1/PL030015A20A02), *cathepsin La/ctsla*
488 (dd_2567_0_1/PL06020B2D09), *piwi-1* (dd_659_0_1/PL06008A2C06), *tgs-1* (dd_10988_0_1),
489 *solute carrier family 22 member 6/slc22a6* (dd_1159_0_1), and Niemann-Pick type C-2/*npc2*
490 (dd_73_0_1/PL030001B20C07). *S. mediterranea ldlr-1, ldlr-2,* and *vldlr-1* were identified by

491 BLAST homology and named after their top human refseq_protein BLASTX hits. Specific
492 sequences of primers and expressed sequence tags (Zayas et al., 2005) will be published in the
493 peer-reviewed manuscript.
494
495 **Domain organization and phylogenetic analysis**
496 For ApoB-1, ApoB-2, Ldlr-1, Ldlr-2, and Vldrl-1, protein domains were identified using
497 HMMSCAN (https://www.ebi.ac.uk/Tools/hmmer/search/hmmscan) to search Pfam, TIGRFAM,
498 and Superfamily databases, with Phobius for transmembrane and signal peptide predictions (E-
499 value cutoff of 1e-03) (Potter et al., 2018). For the ApoB phylogenetic tree, N-terminal
500 Vitellogenin domains from ApoB and related proteins were aligned in Geneious using MUSCLE
501 (default settings), and alignment was trimmed in Gblocks
502 (http://molevol.cmima.csic.es/castresana/Gblocks_server.html) selecting all "less stringent"
503 criteria. Phylogenetic tree was generated using PhyML 3.0 (http://www.atgc-
504 montpellier.fr/phyml/), using AIC for automatic selection of the LG substitution model, BioNJ
505 starting tree, NNI for tree topology improvement, and 100 bootstrap replicates. Accession
506 numbers for proteins used in domain diagrams and phylogenetic analysis will be included in the
507 peer-reviewed manuscript.
508
509 **In situ hybridization**
510 Riboprobe synthesis, WISH, and FISH were conducted as previously described
511 (Forsthoefel et al., 2020). Riboprobes were used at 0.05-1 ng/μl. Cryosections were generated
512 after FISH as in (Forsthoefel et al., 2014).
513
514 **RNAi**
515 dsRNA synthesis and RNAi experiments were conducted as described (Rouhana et al.,
516 2013; Forsthoefel et al., 2020) by mixing one μg of in vitro-synthesized dsRNA with 8-9 μl of

517 1:10 food coloring:water mix, and 40 μl of 2:1 liver:water homogenate. For *nkx2.2* RNAi, animals
518 were fed only once; RNA was extracted for RNA-Seq after seven days. For *apob* RNAi, 2 μg
519 control *egfp* dsRNA or 1 μg each *apob-1* and *apob-2* (for simultaneous RNAi) were mixed with
520 liver and food coloring, and animals were fed 5 times for initial viability experiments, and 3-5
521 times for most other experiments, separating animals with "mild" (*apob-M)* and "severe" *(apob-*
522 *S)* phenotypes prior to fixation, amputation, or flow cytometry. Non-eating planarians were
523 always removed from the experiment if they refused a second dsRNA feeding one day later.
524

525 **pH3-PS10 immunolabeling**

526 Mucus removal and fixation were conducted with 2% ice-cold HCl (3 min) and
527 methacarn (RT, 20 min), followed by bleaching in 6% H_2O_2 in methanol as in (Forsthoefel et al.,
528 2014). Fixed animals/regenerates were blocked (4 hr, RT) in IF block (1X PBS, 0.45% fish
529 gelatin, 0.6% IgG-free BSA, 0.3% Triton X-100), incubated in rabbit anti-phospho-Histone H3-
530 S10 at 1:2000 (O/N, 4°C) (Cell Signaling 3377S), washed 8X in PBSTx (1X PBS plus 0.3%
531 Triton X-100) (30 min each, RT), re-blocked for 1 hr, then incubated with goat anti-rabbit-HRP
532 (1:2000) (Jackson Immuno 111-035-003) (O/N, 4°C). Samples were again washed 8X (20-30
533 min each, RT), then tyramide signal amplification (TSA) was conducted for 20 min as described
534 (King and Newmark, 2013) with TAMRA-tyramide. Samples were washed in PBSTx for two
535 days, then mounted in Vectashield (Vector Labs H-1000-10).
536

537 **Immunolabeling (cryosections)**

538 Cryosections (12 μm) of planarians relaxed in 0.66M $MgCl_2$ and fixed overnight (4°C) in
539 4% formaldehyde (EM)/1X PBS were generated as in (Forsthoefel et al., 2014). After
540 rehydration, heat-mediated antigen retrieval (10 min) in 10 mM sodium citrate, pH 6.0 was
541 performed. Slides were permeabilized for 30 min in 1X PBS/0.2% Tween-20, then blocked for

542 30 min with 0.45% fish gelatin and 0.6% BSA for 30 min in PBSTw (1X PBS, 0.05% Tween 20).
543 incubated with custom rabbit anti-ApoB-1 (1:1000 in block) and mouse 6G10 anti-muscle (1:250
544 in block) (Ross et al., 2015) (ON, 4°C). Slides were washed 3 times (10 min, RT) with PBSTw
545 after each antibody incubation. Slides were then incubated with goat anti-rabbit-HRP (1:2000)
546 (Jackson Immunoresearch, 111-035-144), goat anti-mouse-488 (1:250), and DAPI (2 μg/ml) for
547 15 min at RT. TSA was conducted for 10 min with TAMRA-tyramide as in (King and Newmark,
548 2013). After washing, slides were mounted in Fluoromount G (Southern Biotech).
549

550 **Anti-ApoB-1 antibody generation**

551 Sequence corresponding to the N-terminal Vitellogenin domain of ApoB-1 (dd_636,
552 nucleotides 45-1919, amino acids 1-625) was supplied to GenScript USA (Piscataway, NJ).
553 GenScript synthesized a plasmid encoding this region fused to KLH and a HIS tag, expressed
554 and purified the fusion protein, immunized New Zealand rabbits, affinity purified the antibody,
555 and assessed antibody titer and immunogenicity with both ELISA and Western blot.
556

557 **Protein extraction and Simple Western analysis**

558 5-10 planarians were rocked gently (40-50 rpm) for 7 min in 7.5% N-Acetyl-L-Cysteine
559 and rinsed 2X in 1X PBS. Samples were then homogenized using a motorized Kontes pestle
560 grinder in 250 μl RIPA (50 mM Tris pH 8.0, 150 mM NaCl, 1% NP-40, 0.5% sodium
561 deoxycholate, 0.5% SDS) with 40 mM DTT and 1X Halt Protease Inhibitor cocktail (Thermo
562 Scientific 78430). After 30 min on ice, samples were centrifuged (20,817 x *g,* 15 min, 4°C), and
563 supernatant was recovered and stored at -80°C. DTT concentration was reduced by buffer
564 exchange with RIPA (1 mM DTT) using Amicon Ultra 3 kDa columns (UFC500396), then protein
565 concentration was determined using a BCA kit (Pierce 23225) and DeNovix cuvet
566 spectrophotometer according to manufacturers' protocols. For Simple Western (ProteinSimple),

567 lysates were run according to the manufacturer's protocol on a Wes Instrument (running
568 Compass v4.0.0) at 0.1 mg/ml using the 66-440 kDa Wes Separation module (SM-W008) with
569 anti-ApoB-1 at 1:250 (~2.3 μg/ml). ApoB-1 peak areas were calculated with the following
570 settings: Range 10-600; Baseline Threshold 1.0, Window 15.0, and Stiffness 1.0; and Peak Find
571 Threshold 10.0 and Width 20.0 using the "Dropped Lines" method. Settings were identical for
572 total protein peak area, with these exceptions: Baseline Window 50.0 and Stiffness 0.5.
573 For the regeneration time course, ApoB-1 protein levels were run in biological triplicates,
574 normalized to total protein using the Wes Total Protein Detection Module (DM-TP01), and then
575 normalized to the "0 hour" time point. Statistical analysis was conducted in Prism 9.
576
577 **Oil Red O staining**
578 Planarians were relaxed in 0.66 M $MgCl_2$, fixed overnight (RT) in 4% formaldehyde (EM
579 grade) in 1X PBS, protected in sucrose, and cryosectioned (20 μm) onto SuperFrost Plus slides
580 (Forsthoefel et al., 2014). Slides were rehydrated in deionized (DI) water (3 x 10 min, RT), then
581 stained in Oil Red O (Sigma O0625) solution (6 ml Whatman-filtered 0.5% Oil Red O in 100%
582 isopropanol plus 4 ml ultrapure water) for 15 min at RT. Slides were quickly dipped 3-5X in 60%
583 isopropanol to remove excess dye, then rinsed for 1 min in 60% isopropanol, then rinsed 1 min
584 in DI water. Slides were then rinsed in PBS-Tween-20 (0.01%, to prevent drying), then mounted
585 in 90% glycerol/1X PBS, and imaged within 2-3 days.
586
587 **Thin Layer Chromatography**
588 Ten planarians (5-8 mm) were placed in 1.7 ml microcentrifuge tubes with all planarian
589 salts removed, and the animals' mass was obtained. Lipids were then extracted using the Folch
590 method (Folch and Lees, 1951). Briefly, 1 ml ice-cold 2:1 chloroform:methanol was added, then
591 animals were sonicated in ice water in a cup-horn sonicator (10 cycles of 5 second pulses at

592 ~48-55W). Samples were rocked at RT for 5 hr, then centrifuged (2 min at 16,000 x *g,* 4°C) to
593 pellet insoluble material. Supernatant was recovered to a new tube and stored at -80°C. 1 ml
594 2:1 chloroform:methanol was added to the pellet, re-sonicated, rocked overnight at RT, then
595 centrifuged as above. 0.2 volumes 0.9% NaCl (in water) was added to each extract, tubes were
596 inverted gently 10-15X to mix, vortexed for 10-15 sec, then centrifuged (2 min at 2,000 x *g,* RT).
597 Lower phases from each biological replicate (4 control and 4 *apob(RNAi)* replicates, 10 animals
598 each) were recovered, and speed-vacuumed (30°C x 60-90 min with spinning) to evaporate
599 solvent. Concentrated lipids were resuspended in 2 μl chloroform per mg animal mass (above)
600 and stored at -80°C (for less than 7 days). TLC was performed as in (Carten et al., 2011) with
601 slight modifications. 150Å silica gel HL 250 μl 20x20 cm plates (iChromatography 66011/Miles
602 Scientific P76011) were pre-equilibrated with 1:1 chloroform:methanol (~ 1 hr). After drying, 1 μl
603 lipids and 3 μl standards (30 μg mono-, di-, triglyceride mix, SUPELCO 1787-1AMP, plus 30 μg
604 cholesteryl palmitate, SIGMA C6072) were spotted onto the plates using TLC spotting
605 capillaries. Non-polar lipids were resolved with a 80:10:1 petroleum ether:ethyl ether:acetic acid
606 mix. After drying, TLC plates were sprayed with Primuline (SIGMA 206865) (1 mg/ml fresh stock
607 in ultrapure water, diluted 1:100 into 80 ml acetone plus 20 ml ultrapure water), dried, and
608 imaged on an Alpha Innotech chemiluminescent imager with Cy2 excitation/emission filters.
609 Peak areas in images were quantified in ImageJ/Fiji using the "Plot Lanes" function in the Gels
610 submenu (https://imagej.nih.gov/ij/docs/menus/analyze.html). Averages were calculated and
611 normalized in Excel; statistical analysis was conducted in Prism 9.
612
613 **RNA extraction, library preparation, and RNA sequencing**
614 Uninjured planarians and regenerating tissue fragments were homogenized in Trizol
615 using a motorized Kontes pestle grinder, and RNA was extracted using two chloroform
616 extractions and high-salt precipitation buffer according to the manufacturer's instructions. After

617 precipitation, solutions were transferred to Zymo RNA columns for DNAse treatment and
618 purification, according to manufacturer's instructions. RNA samples were analyzed using Agilent
619 RNA ScreenTape on an Agilent TapeStation 2200 according to manufacturer's protocol.
620 For analysis of gene expression in control vs. *nkx2.2(RNAi),* single-end (75 bp) libraries
621 were generated using the Lexogen Quantseq 3' mRNA Library Prep Kit as previously described,
622 except that sequence was generated with an Illumina NovaSeq 6000 instrument (Forsthoefel et
623 al., 2020). 32M-39M reads were generated for 3 biological replicates per condition. For analysis
624 of gene expression in control, *apob-M,* and *apob-S* animals, total RNA for 4-6 biological
625 replicates per condition was submitted to GENEWIZ (South Plainfield, NJ) for paired-end (2x150
626 bp) library generation using the NEB NEXT ULTRA library prep for standard RNA Seq with
627 standard Illumina adapters. Sequencing was conducted on an Illumina HiSeq instrument; 19M -
628 26M reads were generated for each replicate.
629
630 **Read mapping**
631 For *nkx2.2(RNAi)*, quality control and read mapping were conducted with FastQC
632 (v0.11.5) (Andrews, 2010), BBDuk (v35.66) (https://sourceforge.net/projects/bbmap/), Bowtie2
633 (v2.3.1) (Langmead and Salzberg, 2012), and Samtools (v1.3) (Li et al., 2009) to unique
634 transcripts in dd_Smed_v6 (Brandl et al., 2016) as previously described (Forsthoefel et al.,
635 2020). Similar methods were used for *apob(RNAi)* reads, with several exceptions as follows.
636 BBDUK (v36.99) settings for paired end reads: k=13 ktrim=r mink=11 qtrim=rl trimq=10
637 minlength=35 tbo tpe. Bowtie2 (v2.3.1) for paired end reads was used for mapping, with "-a"
638 multi-mapping and "--local" soft-clipping allowed. For read summarization, the "featureCounts"
639 utility in the Subread package (v1.6.3) (Liao et al., 2019) was used with a custom ".SAF" file and
640 options "-p -M -O -F SAF" to include multi-mapping and multi-overlapping reads.
641 For mapping of X1/X2/Xins, PIWI-HI/-LO/-NEG bulk neoblast transcriptome and
642 regeneration fragment data (Zeng et al., 2018), short read fastq files were downloaded from

643 NCBI GEO (GSE107874), and mapped to dd_Smed_v6_unique with the same settings used for
644 our *nkx2.2(RNAi)* data set.
645
646 **Differential expression analysis**
647 Read counts matrices were imported into R, then analyzed in edgeR v3.8.6 (Robinson et
648 al., 2010). First, all transcripts with counts per million (CPM) < 1 in 3/12 samples (*nxk2.2(RNAi)*
649 and X1/X2/Xins data) or 4/12 samples (all others) (e.g., lowly expressed transcripts) were
650 excluded from further analysis. Next, after recalculation of library sizes, samples were
651 normalized using trimmed mean of M-values (TMM) method, followed by calculation of
652 common, trended, and tagwise dispersions. Finally, differentially expressed transcripts were
653 identified using the pairwise exact test (*nkx2.2(RNAi)* and *apob(RNAi)* experiments) or the
654 generalized linear model (GLM) likelihood ratio test (Zeng data sets). Expression changes were
655 considered to be significant if the false discovery rate adjusted *p* value ("FDR") was <.05.
656
657 **Gene Ontology analysis**
658 GO analysis was conducted using BiNGO (Maere et al., 2005) using a custom *S.*
659 *mediterranea* GO annotation as previously described (Forsthoefel et al., 2020). RefSeq protein
660 collections used for BLASTX and UniProtKB Biological Process GO terms used for annotation
661 were downloaded for each organism in April 2020.
662
663 **Hierarchical clustering and heat maps**
664 Hierarchical clustering of transcripts annotated with lipid-metabolism-related GO terms
665 was conducted using EdgeR-generated $\log_2$FC values in Cluster 3.0 (de Hoon et al., 2004), with
666 Euclidean distance and complete linkage. Heat maps were generated with Java Treeview
667 (Saldanha, 2004).
668

669 **qRT-PCR**

670 Total RNA was extracted from biological triplicates (5-10 animals/fragments per
671 replicate) using Trizol as for RNA-Seq samples. RNA was reverse transcribed using the iScript
672 cDNA Synthesis kit (BioRad 1708890). *apob-1* and *apob-2* levels were detected using the Fast
673 Start Essential Green DNA master mix (Roche 06924204001) on a Roche LightCycler 96
674 instrument. RNA levels were normalized to the geometric mean of endogenous controls *ef-2*
675 and *gapdh* using the Livak ΔΔCt method (Livak and Schmittgen, 2001). Statistical significance
676 was calculated in Microsoft Excel.

677

678 **Flow cytometry**

679 Planarians were dissociated and filtered in CMFB with collagenase as in (van
680 Wolfswinkel et al., 2014). Cells were labeled at RT with Hoechst 33342 (50 μg/ml) for 45 min,
681 followed by addition of propidium iodide (1 μg/ml). For neutral lipid labeling, BODIPY 493/503
682 (Molecular Probes D3922) at 10 ng/ml was included with Hoechst. Cells were analyzed on a
683 Becton Dickinson FACSCelesta instrument with 405 nm, 488 nm, and 640 nm lasers. X1, X2,
684 and Xins gates were drawn using two criteria: cell proportions were approximately 15% (X1)
685 25% (X2) and 60% (Xins), and reductions in X1 and X2 fractions in 4-day post-irradiation
686 animals were >95% and ~70%, respectively. Data were analyzed and plots were generated in
687 FloJo (v10.7.1), and statistical analyses were conducted in Prism 9. For irradiation, uninjured
688 planarians were dosed with 60 Grays (6,000 rads) using RS-2000 Biological Research X-Ray
689 Irradiator (Rad Source, Buford, GA).

690

691 **Cross-referencing of *apob(RNAi)* RNA-Seq data with published transcriptomes**

692 For comparison of dysregulated transcripts in *apob-M* and *apob-S* animals with bulk
693 neoblast transcriptome data (Zeng et al., 2018), we first identified "signature" transcripts as

694 follows. “X1 signature” transcripts were defined as those with a $log_2FC>1$ (FDR<.05) compared
695 to both “X2” and “Xins.” “X2 signature” transcripts had $log_2FC>1$ (fdr<.05) vs. both “X1” and
696 “Xins.” “Xins signature” had $log_2FC>1$ (fdr<.05) vs. both “X1” and “X2.” Similarly, "PIWI-HI
697 signature" transcripts were defined as those with a $log_2FC>1$ (fdr<.05) compared to both "PIWI-
698 LO" and "PIWI-NEG." "PIWI-LO signature" transcripts had $log_2FC>1$ (fdr<.05) vs. both “PIWI-HI”
699 and “PIWI-NEG.” "PIWI-NEG signature" transcripts had $log_2FC>1$ (fdr<.05) vs. both “PIWI-HI”
700 and “PIWI-LO.” Next, we used the "merge" function and "VennDiagram" package in RStudio
701 (v1.2.1335) to identify signature transcripts in X1/X2/Xins or PIWI-HI/-LO/-NEG that were also
702 dsyregulated (up or down) in *apob-M* or *apob-S* animals, as shown in Fig. S5. "% of
703 dysregulated transcripts" was calculated as the number of overlapping transcripts divided by the
704 total number of X1/X2/Xins or PIWI-HI/-LO/-NEG transcripts.
705 For comparison of dysregulated transcripts in *apob-M* and *apob-S* animals with single
706 cell type/state data in (Fincher et al., 2018), we again used the "merge" function in RStudio to
707 identify the number of transcripts enriched in individual lineage subclusters (Table S2) (Fincher
708 et al., 2018) that were also dysregulated by *apob* RNAi. "% of dysregulated transcripts" was
709 calculated as the number of overlapping transcripts divided by the total number of transcripts in
710 each individual subcluster. In Fig. 5, the "N/TS" (Neoblast/Transition State) designation includes
711 subclusters with high *piwi-1* mRNA expression thought to be neoblast/progenitor subpopulations
712 in epidermal, intestine, and protonephridia lineages based on the conclusions of Fincher et al.
713 and other published data (Scimone et al., 2011; Wagner et al., 2011; van Wolfswinkel et al.,
714 2014; Thi-Kim Vu et al., 2015). Similarly, the "P" (Progeny) and "M" (Mature) designations are
715 based on conclusions from both single cell RNA-Seq data and previous work. For lineages that
716 are less well understood *in vivo* (Fig. S6), we designated subclusters with the highest *piwi-1*
717 mRNA levels in t-SNE plots (Fincher et al., 2018) as "N/TS," the most peripheral subclusters
718 (generally with negligible *piwi-1* mRNA levels) as "M", and all other subclusters (with
719 intermediate to low *piwi-1* mRNA levels) as "P."

720

721 **Image Collection and Quantification**

722 Epifluorescent images (FISH samples) were collected on a Zeiss AxioObserver.Z1 with
723 Excelitas X-Cite 120 LED Boost illumination and Zen 2.3 pro. For quantification of pharynx and
724 brain size, organ area and animal area were measured in ImageJ (Schneider et al., 2012) and
725 organ-to-body size ratios were calculated. For intestine, length of anterior branch and posterior
726 branches were measured in ImageJ. Means of posterior branch length were calculated, and
727 then posterior-to-anterior (head fragments) or anterior-to-posterior (tail fragments) length ratio
728 was calculated. For tail fragments, the "split" anterior branch phenotype (failure to fuse at the
729 midline) was scored if there was an obvious gap between anterior branches for at least half the
730 length of the anterior branch. For images of *apob-1* and *apob-2* FISH on cryosections, z-stacks
731 were collected with an Apotome.2 for generation of maximum orthogonal projections. Statistical
732 analysis was conducted in Prism 9.

733 For anti-pH3-PS10-labeled samples, z-stacks were collected on a Zeiss
734 AxioObserver.Z1 at 10X magnification, followed by tile stitching, extended depth of focus
735 projection, and background subtraction (PS10 channel only) with a radius of 30. Control and
736 experimental samples to be compared were imaged at identical exposures. For quantification,
737 animal area and PS10+ nuclei were quantified using the Automated Segmentation tools in Zen
738 2.3 pro. Briefly, animal area was measured with Gaussian smoothing, no background
739 subtraction or sharpening, Morphology separation, and custom threshold settings that were the
740 same for all samples to be directly compared. PS10+ nuclei number was measured using
741 Lowpass smoothing, Rolling Ball background subtraction, Delineate sharpening, Watersheds
742 separation, with threshold settings and other parameters that were identical for all samples to be
743 directly compared. Number of mitoses per area were calculated for each animal/fragment,
744 followed by statistical analyses in Prism 9.

745 Confocal images were collected on a Zeiss LSM 710 or LSM 880 laser scanning
746 microscope with 10X Plan NeoFluar, 20X Plan Apo, or 40X C-Apo objectives. For orthogonal
747 projections (anti-ApoB1 immunolabeling and *ldlr/vldlr* FISH), between three and ten z-planes
748 were collected at 1-2X "optimal" section thickness (based on objective NA). For *notum* and
749 *wnt11-2* FISH, full fragment thickness stacks were projected to ensure counting of all mRNA-
750 positive cells.
751 Images of Oil-Red-O-stained sections, live animals, live regenerates, and WISH samples
752 were collected on a Zeiss Stemi 508 with an Axiocam 105 color camera, or a Zeiss Axio
753 Zoom.V16 with an Axiocam 105 camera. In some cases brightness and/or contrast were
754 adjusted in Adobe Photoshop to improve signal contrast.
755
756 **Reagents and Primers**
757 Detailed information on reagents and primer sequences will be made available on
758 publication of the peer-reviewed manuscript or by request.
759
760 **Data availability**
761 Raw and processed RNA-Seq data associated with this study will be made available in
762 the NCBI Gene Expression Omnibus (GEO) upon publication.
763
764 **Competing interests**
765 The authors declare no competing financial interests.
766
767

768 ## Acknowledgments

769 We are very grateful to Phil Newmark (HHMI and the Morgridge Institute for Research),
770 in whose laboratory this project was initiated. We thank members of the Newmark and
771 Forsthoefel labs, and OMRF colleagues Pat Gaffney, Linda Thompson, Dean Dawson, and Hui-
772 Ying Lim for insightful discussions. We thank Jochen Rink, James Cleland, and Hanh Vu (Max
773 Planck Institute for Biophysical Chemistry) for sharing planarian protein extraction protocols,
774 and Rachel Roberts-Galbraith (Univ. of Georgia) for *notum* and *wnt11-2* plasmids. We thank
775 Steve Farber (Carnegie Instution for Science) for advice on lipid extraction and TLC, and
776 Jayhun Lee (Morgridge) for collaborative development of planarian lipid analysis protocols. We
777 are grateful to Hadi Maktabi (ProteinSimple) and to OMRF colleagues Summer Wang and Lin
778 Wang for help in developing Wes protocols; and to members of the OMRF Flow Cytometry Core
779 (Jacob Bass and Diana Hamilton), the Imaging and Histology Core, the Clinical Genomics Core,
780 and IT/Research Computing Services for invaluable technical assistance. JRO was supported
781 by the Summer Research Opportunities Program at the University of Illinois at Urbana-
782 Champaign. This work was supported by NIH Centers of Biomedical Research Excellence
783 (COBRE) GM103636 (Project 1 to DJF), and the Oklahoma Medical Research Foundation.
784
785
786

787 # References

788

789 Adell, T., Saló, E., Boutros, M., Bartscherer, K., 2009. Smed-Evi/Wntless is required for β-
790 catenin-dependent and -independent processes during planarian regeneration. Development
791 136, 905-910.

792 Andrews, S., 2010. FastQC: a quality control tool for high throughput sequence data.

793 Betchaku, T., 1967. Isolation of planarian neoblasts and their behavior in vitro with some
794 aspects of the mechanism of the formation of regeneration blastema. J Exp Zool 164, 407-433.

795 Brandl, H., Moon, H., Vila-Farre, M., Liu, S.Y., Henry, I., Rink, J.C., 2016. PlanMine--a mineable
796 resource of planarian biology and biodiversity. Nucleic Acids Res. 44, D764-773.

797 Carten, J.D., Bradford, M.K., Farber, S.A., 2011. Visualizing digestive organ morphology and
798 function using differential fatty acid metabolism in live zebrafish. Dev. Biol. 360, 276-285.

799 Clémot, M., Sênos Demarco, R., Jones, D.L., 2020. Lipid Mediated Regulation of Adult Stem
800 Cell Behavior. Front Cell Dev Biol 8, 115.

801 Cornacchia, D., Zhang, C., Zimmer, B., Chung, S.Y., Fan, Y., Soliman, M.A., Tchieu, J.,
802 Chambers, S.M., Shah, H., Paull, D., Konrad, C., Vincendeau, M., Noggle, S.A., Manfredi, G.,
803 Finley, L.W.S., Cross, J.R., Betel, D., Studer, L., 2019. Lipid Deprivation Induces a Stable,
804 Naive-to-Primed Intermediate State of Pluripotency in Human PSCs. Cell Stem Cell 25, 120-136
805 e110.

806 Cruz, A.L.S., Barreto, E.A., Fazolini, N.P.B., Viola, J.P.B., Bozza, P.T., 2020. Lipid droplets:
807 platforms with multiple functions in cancer hallmarks. Cell Death Dis 11, 105.

808 D'Andrea, S., 2016. Lipid droplet mobilization: The different ways to loosen the purse strings.
809 Biochimie 120, 17-27.

810 de Hoon, M.J., Imoto, S., Nolan, J., Miyano, S., 2004. Open source clustering software.
811 Bioinformatics 20, 1453-1454.

812 Deb, S., Felix, D.A., Koch, P., Deb, M.K., Szafranski, K., Buder, K., Sannai, M., Groth, M.,
813 Kirkpatrick, J., Pietsch, S., Gollowitzer, A., Groß, A., Riemenschneider, P., Koeberle, A.,
814 González-Estévez, C., Rudolph, K.L., 2020. Tnfaip2/exoc3-driven lipid metabolism is essential
815 for stem cell differentiation and organ homeostasis. EMBO Rep, e49328.

816 Driver, A.M., Kratz, L.E., Kelley, R.I., Stottmann, R.W., 2016. Altered cholesterol biosynthesis
817 causes precocious neurogenesis in the developing mouse forebrain. Neurobiol Dis 91, 69-82.

818 Eisenhoffer, G.T., Kang, H., Sánchez Alvarado, A., 2008. Molecular analysis of stem cells and
819 their descendants during cell turnover and regeneration in the planarian *Schmidtea*
820 *mediterranea*. Cell Stem Cell 3, 327-339.

821 Fincher, C.T., Wurtzel, O., de Hoog, T., Kravarik, K.M., Reddien, P.W., 2018. Cell type
822 transcriptome atlas for the planarian *Schmidtea mediterranea*. Science 360.

823 Folch, J., Lees, M., 1951. Proteolipides, a new type of tissue lipoproteins; their isolation from
824 brain. J. Biol. Chem. 191, 807-817.

825 Forsthoefel, D.J., Cejda, N.I., Khan, U.W., Newmark, P.A., 2020. Cell-type diversity and
826 regionalized gene expression in the planarian intestine. Elife 9.

827 Forsthoefel, D.J., James, N.P., Escobar, D.J., Stary, J.M., Vieira, A.P., Waters, F.A., Newmark,
828 P.A., 2012. An RNAi screen reveals intestinal regulators of branching morphogenesis,
829 differentiation, and stem cell proliferation in planarians. Dev. Cell 23, 691-704.

830 Forsthoefel, D.J., Park, A.E., Newmark, P.A., 2011. Stem cell-based growth, regeneration, and
831 remodeling of the planarian intestine. Dev. Biol. 356, 445-459.

832 Forsthoefel, D.J., Waters, F.A., Newmark, P.A., 2014. Generation of cell type-specific
833 monoclonal antibodies for the planarian and optimization of sample processing for
834 immunolabeling. BMC Dev. Biol. 14, 45.

835 Gamo, J., Garcia-Corrales, P., 1987. Ultrastructural changes in the gastrodermal phagocytic
836 cells of the freshwater planarian *Dugesia gonocephala* s.l. during starvation. J. Submicrosc.
837 Cytol. 19, 291-302.

838 Gaudet, D., Drouin-Chartier, J.P., Couture, P., 2017. Lipid Metabolism and Emerging Targets
839 for Lipid-Lowering Therapy. Can J Cardiol 33, 872-882.

840 Guo, Y., Cordes, K.R., Farese, R.V., Jr., Walther, T.C., 2009. Lipid droplets at a glance. J. Cell
841 Sci. 122, 749-752.

842 Hayashi, H., Campenot, R.B., Vance, D.E., Vance, J.E., 2004. Glial lipoproteins stimulate axon
843 growth of central nervous system neurons in compartmented cultures. J. Biol. Chem. 279,
844 14009-14015.

845 Hayashi, T., Asami, M., Higuchi, S., Shibata, N., Agata, K., 2006. Isolation of planarian X-ray-
846 sensitive stem cells by fluorescence-activated cell sorting. Dev. Growth Differ. 48, 371-380.

847 Hayashi, T., Shibata, N., Okumura, R., Kudome, T., Nishimura, O., Tarui, H., Agata, K., 2010.
848 Single-cell gene profiling of planarian stem cells using fluorescent activated cell sorting and its
849 "index sorting" function for stem cell research. Dev. Growth Differ. 52, 131-144.

850 Heier, C., Kühnlein, R.P., 2018. Triacylglycerol Metabolism in Drosophila melanogaster.
851 Genetics 210, 1163-1184.

852 Hendzel, M.J., Wei, Y., Mancini, M.A., Van Hooser, A., Ranalli, T., Brinkley, B.R., Bazett-Jones,
853 D.P., Allis, C.D., 1997. Mitosis-specific phosphorylation of histone H3 initiates primarily within
854 pericentromeric heterochromatin during G2 and spreads in an ordered fashion coincident with
855 mitotic chromosome condensation. Chromosoma 106, 348-360.

856 Hussain, M.M., 2014. Intestinal lipid absorption and lipoprotein formation. Curr Opin Lipidol 25,
857 200-206.

858 Ito, K., Carracedo, A., Weiss, D., Arai, F., Ala, U., Avigan, D.E., Schafer, Z.T., Evans, R.M.,
859 Suda, T., Lee, C.H., Pandolfi, P.P., 2012. A PML-PPAR-delta pathway for fatty acid oxidation
860 regulates hematopoietic stem cell maintenance. Nat. Med. 18, 1350-1358.

861 Ito, K., Suda, T., 2014. Metabolic requirements for the maintenance of self-renewing stem cells.
862 Nat. Rev. Mol. Cell Biol. 15, 243-256.

863 Jennings, J.B., 1957. Studies on feeding, digestion, and food storage in free-living flatworms
864 (Platyhelminthes: Turbellaria). Biol. Bull. 112, 63-80.

865 Kang, J., Hu, J., Karra, R., Dickson, A.L., Tornini, V.A., Nachtrab, G., Gemberling, M., Goldman,
866 J.A., Black, B.L., Poss, K.D., 2016. Modulation of tissue repair by regeneration enhancer
867 elements. Nature 532, 201-206.

868 King, R.S., Newmark, P.A., 2013. *In situ* hybridization protocol for enhanced detection of gene
869 expression in the planarian *Schmidtea mediterranea*. BMC Dev. Biol. 13, 8.

870 Knobloch, M., Braun, S.M., Zurkirchen, L., von Schoultz, C., Zamboni, N., Arauzo-Bravo, M.J.,
871 Kovacs, W.J., Karalay, O., Suter, U., Machado, R.A., Roccio, M., Lutolf, M.P., Semenkovich,
872 C.F., Jessberger, S., 2013. Metabolic control of adult neural stem cell activity by Fasn-
873 dependent lipogenesis. Nature 493, 226-230.

874 Knobloch, M., Pilz, G.A., Ghesquiere, B., Kovacs, W.J., Wegleiter, T., Moore, D.L., Hruzova, M.,
875 Zamboni, N., Carmeliet, P., Jessberger, S., 2017. A Fatty Acid Oxidation-Dependent Metabolic
876 Shift Regulates Adult Neural Stem Cell Activity. Cell Rep 20, 2144-2155.

877 Lafontan, M., Langin, D., 2009. Lipolysis and lipid mobilization in human adipose tissue. Prog
878 Lipid Res 48, 275-297.

879 Langmead, B., Salzberg, S.L., 2012. Fast gapped-read alignment with Bowtie 2. Nat. Methods
880 9, 357-359.

881 Li, H., Handsaker, B., Wysoker, A., Fennell, T., Ruan, J., Homer, N., Marth, G., Abecasis, G.,
882 Durbin, R., Genome Project Data Processing, S., 2009. The Sequence Alignment/Map format
883 and SAMtools. Bioinformatics 25, 2078-2079.

884 Liao, Y., Smyth, G.K., Shi, W., 2019. The R package Rsubread is easier, faster, cheaper and
885 better for alignment and quantification of RNA sequencing reads. Nucleic Acids Res. 47, e47.

886 Livak, K.J., Schmittgen, T.D., 2001. Analysis of relative gene expression data using real-time
887 quantitative PCR and the 2(-Delta Delta C(T)) Method. Methods 25, 402-408.

888 Love, N.R., Ziegler, M., Chen, Y., Amaya, E., 2014. Carbohydrate metabolism during vertebrate
889 appendage regeneration: what is its role? How is it regulated?: A postulation that regenerating
890 vertebrate appendages facilitate glycolytic and pentose phosphate pathways to fuel
891 macromolecule biosynthesis. Bioessays 36, 27-33.

892 Ly, C.H., Lynch, G.S., Ryall, J.G., 2020. A Metabolic Roadmap for Somatic Stem Cell Fate. Cell
893 Metab 31, 1052-1067.

894 Maere, S., Heymans, K., Kuiper, M., 2005. BiNGO: a Cytoscape plugin to assess
895 overrepresentation of gene ontology categories in biological networks. Bioinformatics 21, 3448-
896 3449.

897 Mak, H.Y., 2012. Lipid droplets as fat storage organelles in Caenorhabditis elegans: Thematic
898 Review Series: Lipid Droplet Synthesis and Metabolism: from Yeast to Man. J. Lipid Res. 53,
899 28-33.

900 Monnot, M.J., Babin, P.J., Poleo, G., Andre, M., Laforest, L., Ballagny, C., Akimenko, M.A.,
901 1999. Epidermal expression of apolipoprotein E gene during fin and scale development and fin
902 regeneration in zebrafish. Dev. Dyn. 214, 207-215.

903 Newmark, P.A., Sánchez Alvarado, A., 2000. Bromodeoxyuridine specifically labels the
904 regenerative stem cells of planarians. Dev. Biol. 220, 142-153.

905 Newmark, P.A., Sánchez Alvarado, A., 2002. Not your father's planarian: a classic model enters
906 the era of functional genomics. Nat. Rev. Genet. 3, 210-219.

907 Olofsson, S.O., Asp, L., Borén, J., 1999. The assembly and secretion of apolipoprotein B-
908 containing lipoproteins. Curr Opin Lipidol 10, 341-346.

909 Olofsson, S.O., Borén, J., 2005. Apolipoprotein B: a clinically important apolipoprotein which
910 assembles atherogenic lipoproteins and promotes the development of atherosclerosis. J Intern
911 Med 258, 395-410.

912 Olzmann, J.A., Carvalho, P., 2019. Dynamics and functions of lipid droplets. Nat. Rev. Mol. Cell
913 Biol. 20, 137-155.

914 Pala, F., Di Girolamo, D., Mella, S., Yennek, S., Chatre, L., Ricchetti, M., Tajbakhsh, S., 2018.
915 Distinct metabolic states govern skeletal muscle stem cell fates during prenatal and postnatal
916 myogenesis. J. Cell Sci. 131.

917 Palm, W., Rodenfels, J., 2020. Understanding the role of lipids and lipoproteins in development.
918 Development 147.

919 Palm, W., Sampaio, J.L., Brankatschk, M., Carvalho, M., Mahmoud, A., Shevchenko, A., Eaton,
920 S., 2012. Lipoproteins in Drosophila melanogaster--assembly, function, and influence on tissue
921 lipid composition. PLoS Genet. 8, e1002828.

922 Panáková, D., Sprong, H., Marois, E., Thiele, C., Eaton, S., 2005. Lipoprotein particles are
923 required for Hedgehog and Wingless signalling. Nature 435, 58-65.

924 Pauta, M., Rotllan, N., Vales, F., Fernandez-Hernando, A., Allen, R.M., Ford, D.A., Mari, M.,
925 Jiménez, W., Baldán, Á., Morales-Ruiz, M., Fernández-Hernando, C., 2013. Impaired liver
926 regeneration in Ldlr-/- mice is associated with an altered hepatic profile of cytokines, growth
927 factors, and lipids. J Hepatol 59, 731-737.

928 Petersen, C.P., Reddien, P.W., 2011. Polarized notum activation at wounds inhibits Wnt
929 function to promote planarian head regeneration. Science 332, 852-855.

930 Potter, S.C., Luciani, A., Eddy, S.R., Park, Y., Lopez, R., Finn, R.D., 2018. HMMER web server:
931 2018 update. Nucleic Acids Res. 46, W200-W204.

932 Reddien, P.W., 2018. The Cellular and Molecular Basis for Planarian Regeneration. Cell 175,
933 327-345.

934 Reddien, P.W., Bermange, A.L., Murfitt, K.J., Jennings, J.R., Sánchez Alvarado, A., 2005a.
935 Identification of genes needed for regeneration, stem cell function, and tissue homeostasis by
936 systematic gene perturbation in planaria. Dev. Cell 8, 635-649.

937 Reddien, P.W., Oviedo, N.J., Jennings, J.R., Jenkin, J.C., Sánchez Alvarado, A., 2005b.
938 SMEDWI-2 is a PIWI-like protein that regulates planarian stem cells. Science 310, 1327-1330.

939 Reddien, P.W., Sánchez Alvarado, A., 2004. Fundamentals of planarian regeneration. Annu.
940 Rev. Cell Dev. Biol. 20, 725-757.

941 Rigotti, A., 2007. Absorption, transport, and tissue delivery of vitamin E. Mol Aspects Med 28,
942 423-436.

943 Roberts-Galbraith, R.H., Newmark, P.A., 2013. Follistatin antagonizes Activin signaling and acts
944 with Notum to direct planarian head regeneration. Proc Natl Acad Sci U S A 110, 1363-1368.

945 Robinson, M.D., McCarthy, D.J., Smyth, G.K., 2010. edgeR: a Bioconductor package for
946 differential expression analysis of digital gene expression data. Bioinformatics 26, 139-140.

947 Ross, K.G., Omuro, K.C., Taylor, M.R., Munday, R.K., Hubert, A., King, R.S., Zayas, R.M.,
948 2015. Novel monoclonal antibodies to study tissue regeneration in planarians. BMC Dev. Biol.
949 15, 2.

950 Rouhana, L., Weiss, J.A., Forsthoefel, D.J., Lee, H., King, R.S., Inoue, T., Shibata, N., Agata,
951 K., Newmark, P.A., 2013. RNA interference by feeding in vitro-synthesized double-stranded
952 RNA to planarians: methodology and dynamics. Dev. Dyn. 242, 718-730.

953 Ruggles, K.V., Turkish, A., Sturley, S.L., 2013. Making, baking, and breaking: the synthesis,
954 storage, and hydrolysis of neutral lipids. Annu. Rev. Nutr. 33, 413-451.

955 Saldanha, A.J., 2004. Java Treeview--extensible visualization of microarray data. Bioinformatics
956 20, 3246-3248.

957 Sánchez Alvarado, A., Newmark, P.A., Robb, S.M., Juste, R., 2002. The *Schmidtea*
958 *mediterranea* database as a molecular resource for studying platyhelminthes, stem cells and
959 regeneration. Development 129, 5659-5665.

960 Schneider, C.A., Rasband, W.S., Eliceiri, K.W., 2012. NIH Image to ImageJ: 25 years of image
961 analysis. Nat. Methods 9, 671-675.

962 Scimone, M.L., Meisel, J., Reddien, P.W., 2010. The Mi-2-like *Smed-CHD4* gene is required for
963 stem cell differentiation in the planarian *Schmidtea mediterranea*. Development 137, 1231-1241.

964 Scimone, M.L., Srivastava, M., Bell, G.W., Reddien, P.W., 2011. A regulatory program for
965 excretory system regeneration in planarians. Development 138, 4387-4398.

966 Sênos Demarco, R., Uyemura, B.S., D'Alterio, C., Jones, D.L., 2019. Mitochondrial fusion
967 regulates lipid homeostasis and stem cell maintenance in the Drosophila testis. Nat. Cell Biol.
968 21, 710-720.

969 Shook, B.A., Wasko, R.R., Mano, O., Rutenberg-Schoenberg, M., Rudolph, M.C., Zirak, B.,
970 Rivera-Gonzalez, G.C., López-Giráldez, F., Zarini, S., Rezza, A., Clark, D.A., Rendl, M.,
971 Rosenblum, M.D., Gerstein, M.B., Horsley, V., 2020. Dermal Adipocyte Lipolysis and
972 Myofibroblast Conversion Are Required for Efficient Skin Repair. Cell Stem Cell 26, 880-895
973 e886.

974 Shyh-Chang, N., Daley, G.Q., Cantley, L.C., 2013. Stem cell metabolism in tissue development
975 and aging. Development 140, 2535-2547.

976 Shyh-Chang, N., Ng, H.H., 2017. The metabolic programming of stem cells. Genes Dev. 31,
977 336-346.

978 Sinclair, J.W., Hoying, D.R., Bresciani, E., Nogare, D.D., Needle, C.D., Wu, W., Bishop, K.,
979 Elkahloun, A.G., Chitnis, A., Liu, P., Burgess, S.M., 2020. A metabolic shift to glycolysis
980 promotes zebrafish tail regeneration through TGF–β dependent dedifferentiation of notochord
981 cells to form the blastema. bioRxiv, 2020.2003.2003.975318.

982 Singh, S.R., Zeng, X., Zhao, J., Liu, Y., Hou, G., Liu, H., Hou, S.X., 2016. The lipolysis pathway
983 sustains normal and transformed stem cells in adult Drosophila. Nature 538, 109-113.

984 Tamilarasan, K.P., Temmel, H., Das, S.K., Al Zoughbi, W., Schauer, S., Vesely, P.W., Hoefler,
985 G., 2012. Skeletal muscle damage and impaired regeneration due to LPL-mediated lipotoxicity.
986 Cell Death Dis 3, e354.

987 Thi-Kim Vu, H., Rink, J.C., McKinney, S.A., McClain, M., Lakshmanaperumal, N., Alexander, R.,
988 Sánchez Alvarado, A., 2015. Stem cells and fluid flow drive cyst formation in an invertebrate
989 excretory organ. Elife 4.

990 Thommen, A., Werner, S., Frank, O., Philipp, J., Knittelfelder, O., Quek, Y., Fahmy, K.,
991 Shevchenko, A., Friedrich, B.M., Julicher, F., Rink, J.C., 2019. Body size-dependent energy
992 storage causes Kleiber's law scaling of the metabolic rate in planarians. Elife 8.

993 Tirinato, L., Pagliari, F., Limongi, T., Marini, M., Falqui, A., Seco, J., Candeloro, P., Liberale, C.,
994 Di Fabrizio, E., 2017. An Overview of Lipid Droplets in Cancer and Cancer Stem Cells. Stem
995 Cells Int 2017, 1656053.

996 Tiwari, S.K., Toshniwal, A.G., Mandal, S., Mandal, L., 2020. Fatty acid beta-oxidation is required
997 for the differentiation of larval hematopoietic progenitors in Drosophila. Elife 9.

998 van Wolfswinkel, J.C., Wagner, D.E., Reddien, P.W., 2014. Single-cell analysis reveals
999 functionally distinct classes within the planarian stem cell compartment. Cell Stem Cell 15, 326-
1000 339.

1001 Voss, S.R., Palumbo, A., Nagarajan, R., Gardiner, D.M., Muneoka, K., Stromberg, A.J.,
1002 Athippozhy, A.T., 2015. Gene expression during the first 28 days of axolotl limb regeneration I:
1003 Experimental design and global analysis of gene expression. Regeneration (Oxf) 2, 120-136.

1004 Wagner, D.E., Wang, I.E., Reddien, P.W., 2011. Clonogenic neoblasts are pluripotent adult
1005 stem cells that underlie planarian regeneration. Science 332, 811-816.

1006 Walther, T.C., Chung, J., Farese, R.V., Jr., 2017. Lipid Droplet Biogenesis. Annu. Rev. Cell.
1007 Dev. Biol. 33, 491-510.

1008 Welte, M.A., Gould, A.P., 2017. Lipid droplet functions beyond energy storage. Biochim Biophys
1009 Acta Mol Cell Biol Lipids 1862, 1260-1272.

1010 Wenemoser, D., Reddien, P.W., 2010. Planarian regeneration involves distinct stem cell
1011 responses to wounds and tissue absence. Dev. Biol. 344, 979-991.

1012 Willier, B.H., Hyman, L.H., Rifenburgh, S.A., 1925. A histochemical study of intracellular
1013 digestion in triclad flatworms. Journal of Morphology and Physiology 40, 299-340.

1014 Wong, L.H., Gatta, A.T., Levine, T.P., 2019. Lipid transfer proteins: the lipid commute via
1015 shuttles, bridges and tubes. Nat. Rev. Mol. Cell Biol. 20, 85-101.

1016 Wurtzel, O., Cote, L.E., Poirier, A., Satija, R., Regev, A., Reddien, P.W., 2015. A generic and
1017 cell-type-specific wound response precedes regeneration in planarians. Dev. Cell 35, 632-645.

1018 Zayas, R.M., Hernandez, A., Habermann, B., Wang, Y., Stary, J.M., Newmark, P.A., 2005. The
1019 planarian *Schmidtea mediterranea* as a model for epigenetic germ cell specification: analysis of
1020 ESTs from the hermaphroditic strain. Proc. Natl. Acad. Sci. USA 102, 18491-18496.

1021 Zeng, A., Li, H., Guo, L., Gao, X., McKinney, S., Wang, Y., Yu, Z., Park, J., Semerad, C., Ross,
1022 E., Cheng, L.C., Davies, E., Lei, K., Wang, W., Perera, A., Hall, K., Peak, A., Box, A., Sanchez
1023 Alvarado, A., 2018. Prospectively Isolated Tetraspanin(+) Neoblasts Are Adult Pluripotent Stem
1024 Cells Underlying Planaria Regeneration. Cell 173, 1593-1608 e1520.

1025 Zhang, S., Guo, L., Guerrero-Hernández, C., Ross, E.J., Gotting, K., McKinney, S.A., Wang, W.,
1026 Xiang, Y., Hawley, R.S., Sánchez Alvarado, A., 2018. A nuclear hormone receptor and lipid
1027 metabolism axis are required for the maintenance and regeneration of reproductive organs.
1028 bioRxiv, 279364.

1029 Zhu, S.J., Hallows, S.E., Currie, K.W., Xu, C., Pearson, B.J., 2015. A *mex3* homolog is required
1030 for differentiation during planarian stem cell lineage development. Elife 4, e07025.
1031

1032

1033 **Figures and Figure Legends**

1034

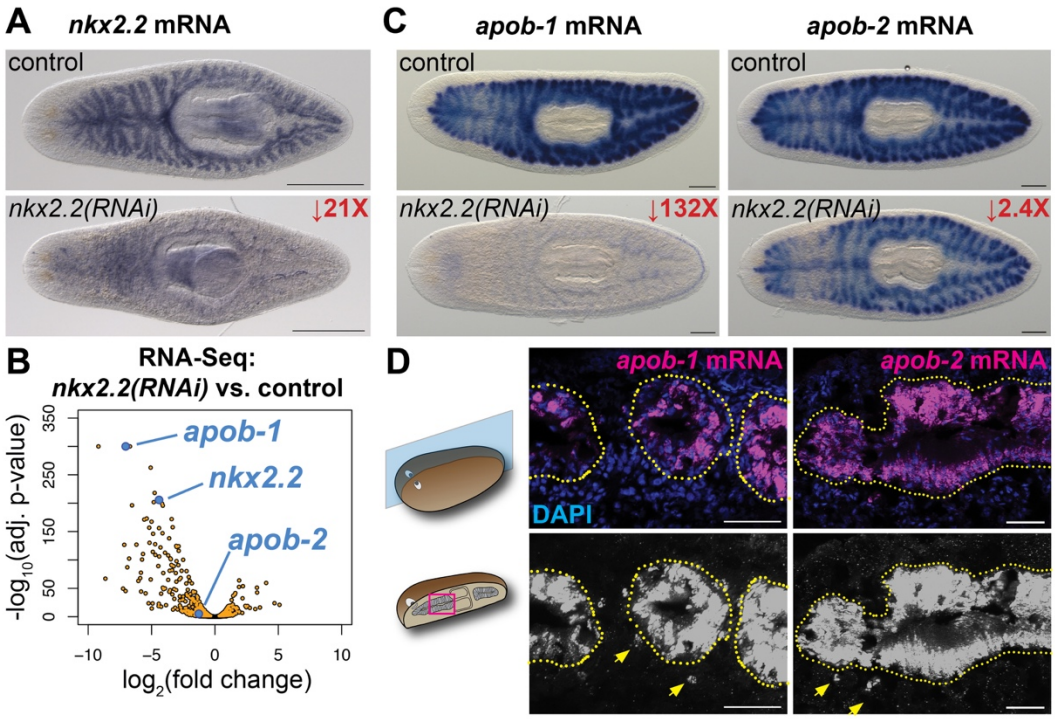

1035 **Figure 1.**

1036 **Figure 1. Transcripts encoding planarian *apolipoprotein b* orthologs are intestine-**
1037 **enriched and downregulated in *nkx2.2(RNAi)* animals. (A)** *nkx2.2* mRNA *in situ* expression
1038 patterns in uninjured control and *nkx2.2(RNAi)* planarians. **(B)** Volcano plot showing
1039 downregulation of *apob-1, apob-2,* and *nkx2.2* in *nkx2.2(RNAi)* animals. An offset of 1e-300 was
1040 added to all FDR values to enable plotting of transcripts with FDR=0. **(C)** *apob-1* and *apob-2*
1041 mRNA (ISH) expression in control (top) and *nkx2.2(RNAi)* planarians. **(D)** *apob-1* and *apob-2*
1042 mRNA expression (FISH) in sagittal sections. Arrows indicate *apob*-expressing cells outside the
1043 intestine (dotted yellow outline) in digitally brightened images. Scale bars: 500 µm **(A)**; 200 µm
1044 **(C)**; 50 µm **(D)**.
1045

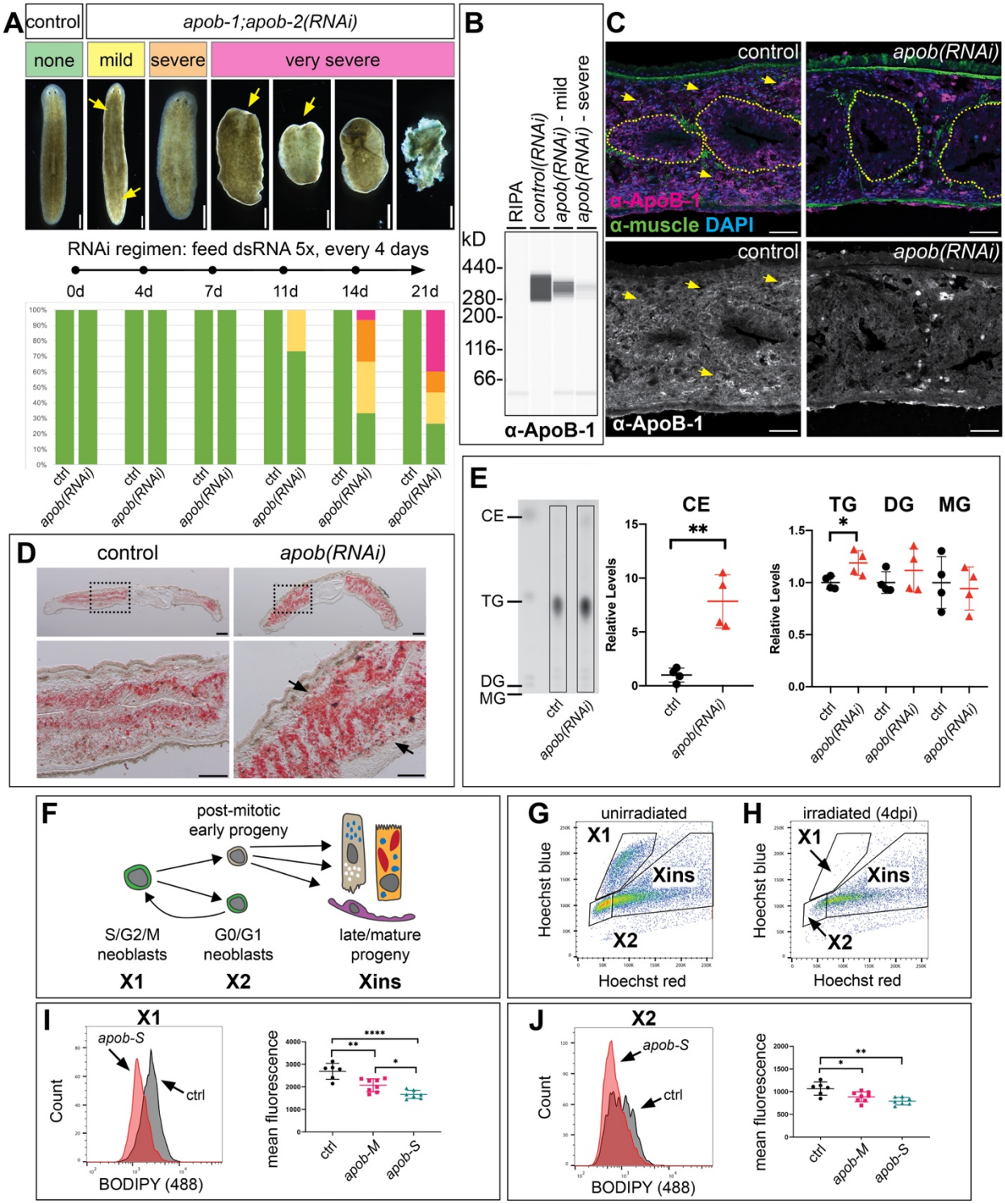
A
control
apob-1;apob-2(RNAi)
none
mild
severe
very severe
RNAi regimen: feed dsRNA 5x, every 4 days
0d
4d
7d
11d
14d
21d
ctrl
apob(RNAi)
B
RIPA
control(RNAi)
apob(RNAi) - mild
apob(RNAi) - severe
kD
440-
280-
200-
116-
66-
α-ApoB-1
C
control
apob(RNAi)
α-ApoB-1
α-muscle DAPI
D
control
apob(RNAi)
E
CE
TG
DG
MG
Relative Levels
F
post-mitotic
early progeny
S/G2/M
neoblasts
X1
G0/G1
neoblasts
X2
late/mature
progeny
Xins
G
unirradiated
Hoechst blue
Hoechst red
H
irradiated (4dpi)
I
Count
BODIPY (488)
mean fluorescence
apob-S
ctrl
apob-M
J

Figure 2.

1049 **Figure 2. *apob* orthologs are required for viability and neutral lipid metabolism. (A)**
1050 Simultaneous RNAi-mediated knockdown of *apob-1* and *apob-2* causes mild (yellow) and
1051 severe (orange) depigmentation, and very severe (pink) phenotypes including head regression,
1052 ventral curling, and lysis. n>10 animals per time point. **(B)** Simple Western (capillary-based
1053 protein analysis) lane view of extracts from control and knockdown planarians labeled with
1054 custom anti-ApoB-1. **(C)** ApoB-1 protein expression in sagittal sections. Expression in intestine
1055 (dotted outline) and outside the intestine (arrows) is dramatically reduced in "very severe" *apob-*
1056 *1(RNAi);apob-2(RNAi)* planarians (right panels). mAb 6G10 (green) labels body wall,
1057 dorsoventral, and visceral muscle fibers (demarcating the intestine.) **(D)** Neutral lipids
1058 accumulate in the intestine and parenchyma (arrows) of "mild" *apob(RNAi)* planarians. Oil Red
1059 O labeling, sagittal sections. **(E)** Cholesteryl esters (CE) and triglycerides (TG), but not
1060 diacylglycerides (DG) or monoglycerides (MG) were significantly elevated in "mild" *apob(RNAi)*
1061 animals. Thin layer chromatography, intensities of lipid species measured in ImageJ and
1062 normalized to controls. n=4, p=.0092 (CE) and p=.0415 (TG), one-way ANOVA, two-stage linear
1063 step-up procedure of Benjamini, Krieger, and Yekutieli. **(F)** Lineage schematic indicating cell
1064 types in X1, X2, and Xins gates on flow cytometry scatter plots. **(G)** Sample flow plot for
1065 uninjured animals. **(H)** Example plot for animals 4 days post irradiation ("4 dpi"), showing
1066 ablation of cells in X1 and depletion of cells in X2. **(I-J)** *apob* knockdown causes reduction of
1067 neutral lipids in X1 and X2 cells. n>6 biological replicates, one-way ANOVA and Tukey's
1068 multiple comparisons test. Scale bars: 50 µm **(C)**; 200 µm **(D,** upper panels**)**; 100 µm **(D,** lower
1069 panels**)**.
1070

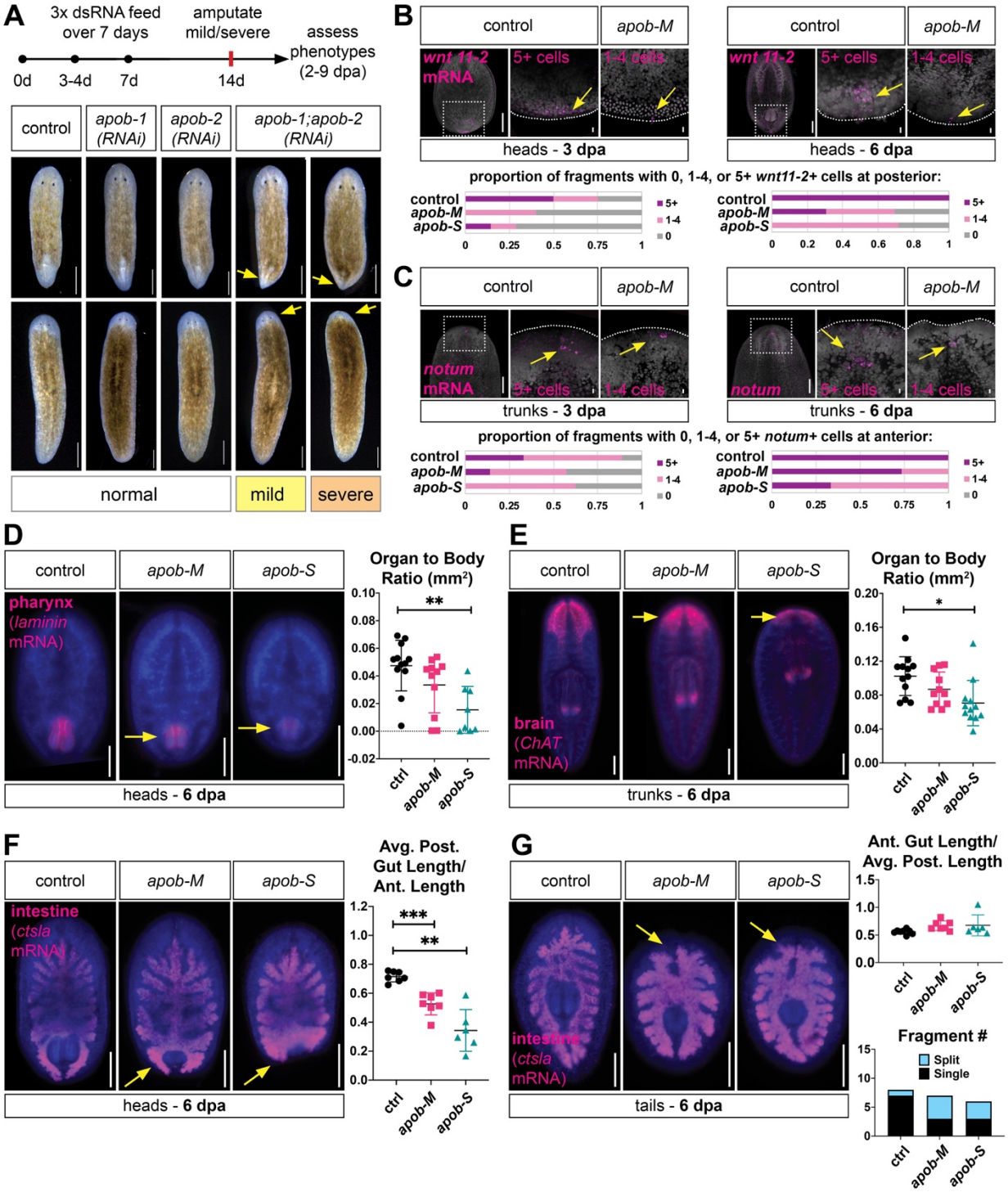
A
3x dsRNA feed over 7 days
amputate mild/severe
assess phenotypes (2-9 dpa)
0d
3-4d
7d
14d
control
apob-1 (RNAi)
apob-2 (RNAi)
apob-1;apob-2 (RNAi)
normal
mild
severe
B
control
apob-M
wnt 11-2 mRNA
5+ cells
1-4 cells
heads - 3 dpa
heads - 6 dpa
proportion of fragments with 0, 1-4, or 5+ wnt11-2+ cells at posterior:
control
apob-M
apob-S
5+
1-4
0
C
notum mRNA
trunks - 3 dpa
trunks - 6 dpa
proportion of fragments with 0, 1-4, or 5+ notum+ cells at anterior:
D
apob-S
pharynx (laminin mRNA)
heads - 6 dpa
Organ to Body Ratio (mm²)
ctrl
E
brain (ChAT mRNA)
trunks - 6 dpa
F
intestine (ctsla mRNA)
Avg. Post. Gut Length/ Ant. Length
G
Ant. Gut Length/ Avg. Post. Length
tails - 6 dpa
Fragment #
Split
Single

Figure 3.

1074 **Figure 3. *apob* inhibition delays regeneration. (A)** *apob* double knockdown results in smaller
1075 blastemas (arrows) in head and trunk regenerates (8 dpa). **(B-C)** Differentiation of cells
1076 expressing polarity genes *wnt11-2* (posterior) and *notum* (anterior) is delayed in *apob(RNAi)*
1077 *animals.* FISH; max projections of confocal images. n=5-15 fragments per condition were
1078 scored for number of positive cells. Control and *apob-M* fragments shown as phenotype
1079 examples. **(D)** Pharynx regeneration is reduced in *apob(RNAi)* head regenerates (6 dpa)
1080 (*laminin* mRNA FISH, epifluorescent images). p=.0021, control vs. *apob-S.* **(E)** CNS
1081 regeneration is reduced in *apob(RNAi)* head regenerates (6 dpa) (*ChAT* mRNA FISH,
1082 epifluorescent images). p=.0101, control vs. *apob-S.* **(F-G)** *apob* RNAi affects intestine
1083 regeneration (6 dpa) (*ctsla* mRNA FISH, epifluorescent images). New branches are shorter in
1084 heads **(F)**. p=.0004 (*apob-M*); p=.0016 (*apob-S*). New branches often fail to fuse in tails **(G)**. All
1085 significance testing: one-way ANOVA (multiple comparisons) with Dunnet's T3 test. DAPI (blue)
1086 in **(D-G)**. Error bars = mean +/- S.D. Scale bars: 500 µm **(A)**; 200 µm **(B-C);** 10 µm **(B-C** insets**);**
1087 200 µm **(D-G)**.
1088

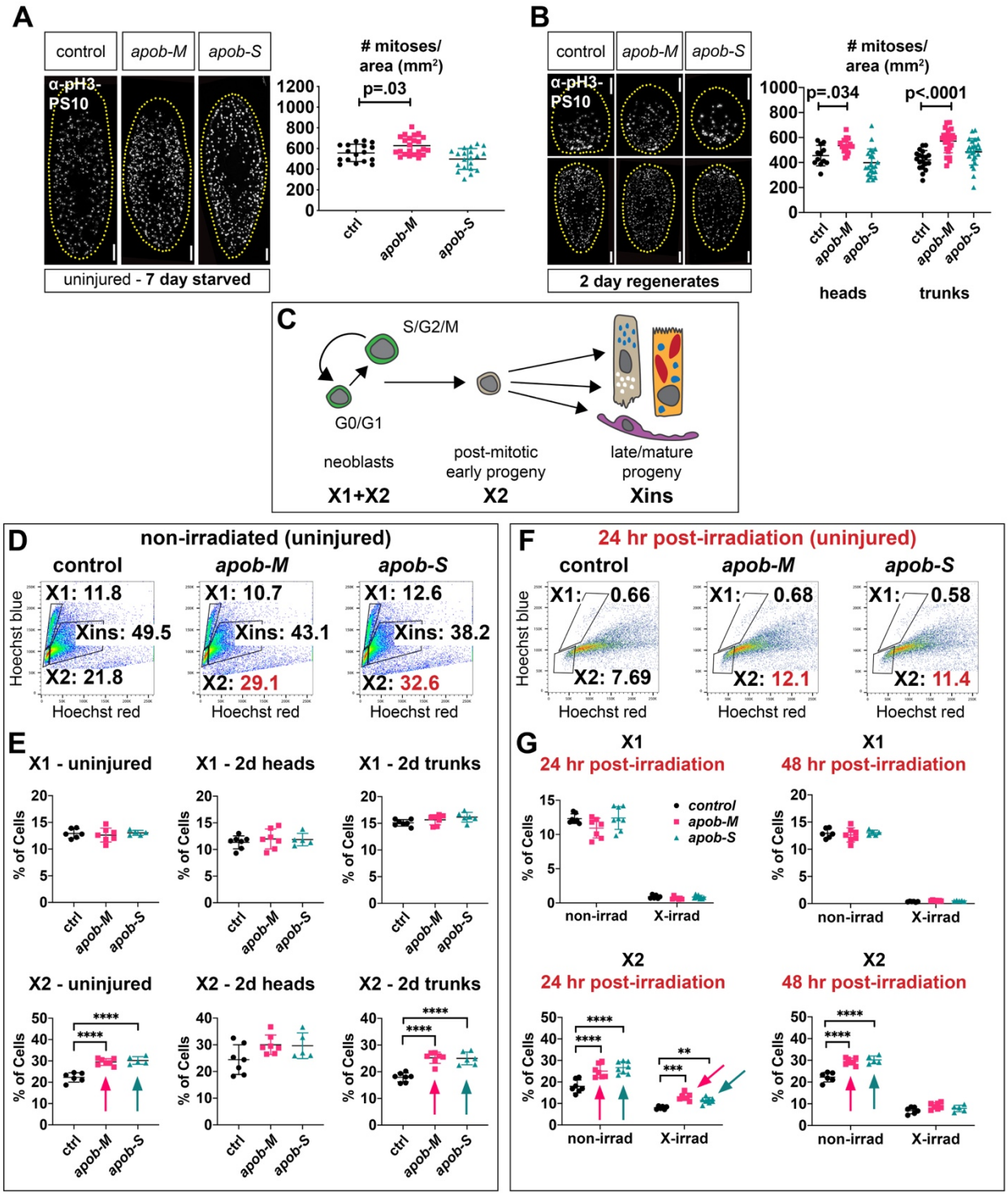
A
control
apob-M
apob-S
α-pH3-PS10
uninjured - 7 day starved
# mitoses/ area (mm²)
p=.03
ctrl
apob-M
apob-S
B
2 day regenerates
p=.034
p<.0001
heads
trunks
C
S/G2/M
G0/G1
neoblasts
X1+X2
post-mitotic early progeny
X2
late/mature progeny
Xins
D
non-irradiated (uninjured)
X1: 11.8
Xins: 49.5
X2: 21.8
X1: 10.7
Xins: 43.1
X2: 29.1
X1: 12.6
Xins: 38.2
X2: 32.6
Hoechst blue
Hoechst red
E
X1 - uninjured
X1 - 2d heads
X1 - 2d trunks
X2 - uninjured
X2 - 2d heads
X2 - 2d trunks
% of Cells
F
24 hr post-irradiation (uninjured)
X1: 0.66
X2: 7.69
X1: 0.68
X2: 12.1
X1: 0.58
X2: 11.4
G
X1
24 hr post-irradiation
48 hr post-irradiation
X2
control
non-irrad
X-irrad

Figure 4.

1093 **Figure 4. *apob* inhibition causes accumulation of neoblast progeny. (A-B)**
1094 phosphoHistone-H3-S10-positive (pH3-PS10) cells are modestly elevated in *apob-M,* but not
1095 *apob-S,* uninjured animals (A) and 2-day regenerates (B). **(C)** Lineage schematic indicating cell
1096 types/states in X1, X2, and Xins gates. **(D)** Examples of flow plots from uninjured planarians
1097 indicating percentages of cells in each gate, with X2 increase in *apob(RNAi)* animals in red. **(E)**
1098 Percentage of cells in X1 and X2 in uninjured (left), 2-day head (middle), and 2-day trunk (right)
1099 regenerates. Arrows indicate significant increases in X2. **(F)** Examples of flow plots from
1100 uninjured planarians, 24 hr post-irradiation, indicating percentages of cells in each gate, with X2
1101 increase in *apob(RNAi)* animals in red. **(G)** Percentage of cells in X1 and X2 in uninjured
1102 planarians, 24 hr (left) and 48 hr (right) post-irradiation. Arrows indicate significant increases in
1103 X2. pH3-PS10 significance testing: one-way ANOVA (multiple comparisons) with Dunnet's T3
1104 test. Flow cytometry significance testing: one-way ANOVA and Tukey's multiple comparisons
1105 test for non-irradiated samples, and two-way ANOVA and two-stage linear step-up procedure of
1106 Benjamini, Krieger and Yekutieli for multiple comparisons for irradiated samples. Error bars =
1107 mean +/- S.D. Scale bars: 200 μm **(A-B)**.
1108

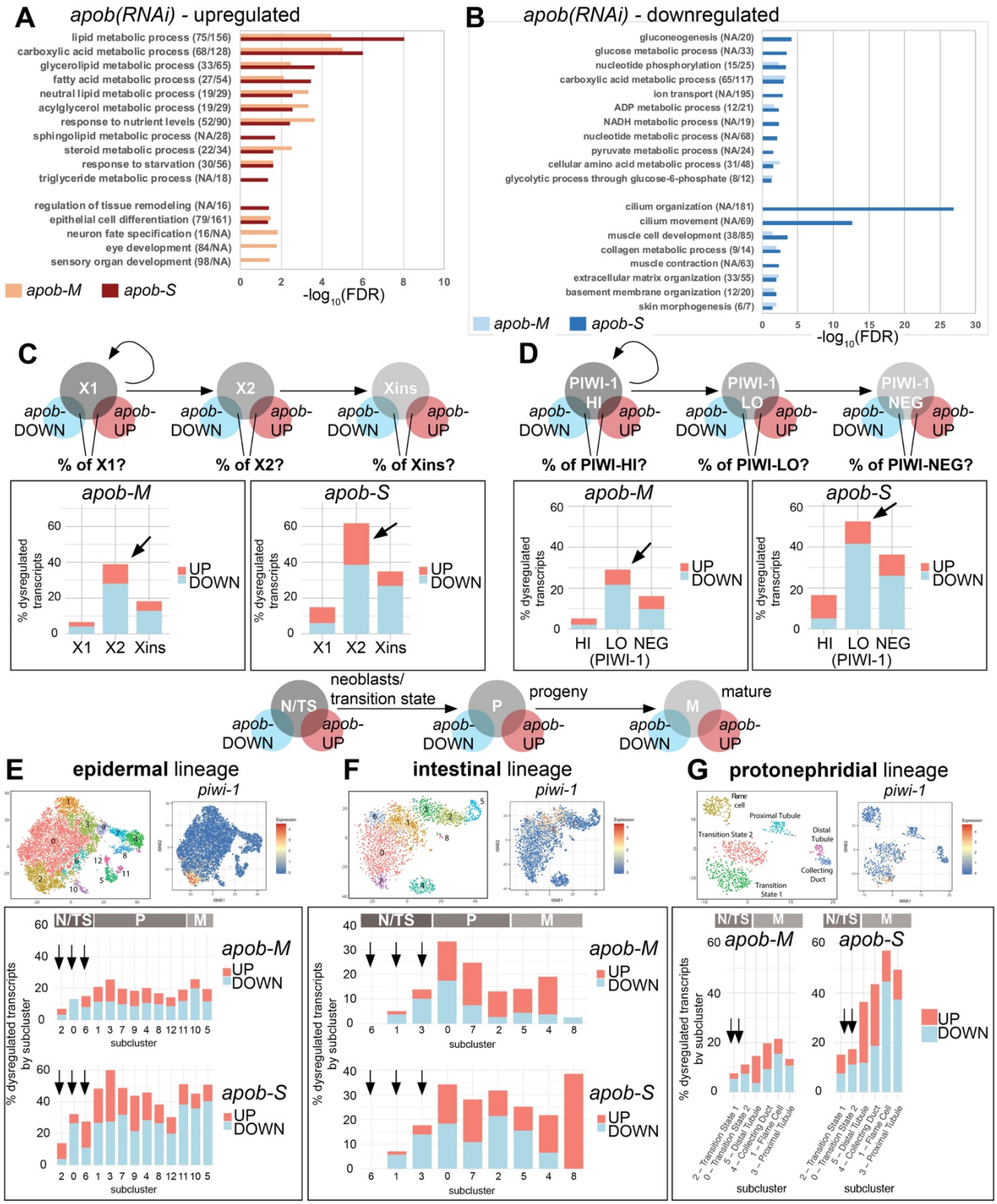

1109

1110

1111 **Figure 5.**

1112 **Figure 5. *apob* RNAi preferentially dysregulates transcripts in differentiating neoblast**
1113 **progeny and mature post-mitotic cells. (A-B)** Gene Ontology Biological Process categories
1114 over-represented among transcripts up- or down-regulated by *apob* RNAi. Numbers of
1115 transcripts dysregulated in (*apob-M/apob-S*); -$\log_{10}$(FDR) on X-axis. **(C-D)** *apob* knockdown
1116 dysregulates greater proportions of X2 and PIWI-LOW signature transcripts (arrows in
1117 histograms). Venn diagrams show analysis scheme: percent of X1/X2/Xins and PIWI-HI/PIWI-
1118 LO/PIWI-NEG signature transcripts that overlap with transcripts dysregulated in *apob-M/apob-S*
1119 animals. Histograms show percentage of signature transcripts up- and down-regulated in *apob-*
1120 *M/apob-S* animals. **(E-G)** *apob* knockdown dysregulates greater proportions of transcripts
1121 enriched in progeny ("P") and mature ("M") post-mitotic cell subclusters in multiple cell type
1122 lineages. Arrows indicate less-affected transcripts enriched in neoblasts/transition state ("N/TS")
1123 subclusters. Venn diagrams show analysis scheme: proportion of subcluster-enriched
1124 transcripts that overlap with transcripts dysregulated in *apob-M/apob-S* animals. t-SNE plots
1125 (digiworm.wi.mit.edu) indicate subclusters and *piwi-1* mRNA expression.
1126

1127

Supplemental Figures and Figure Legends

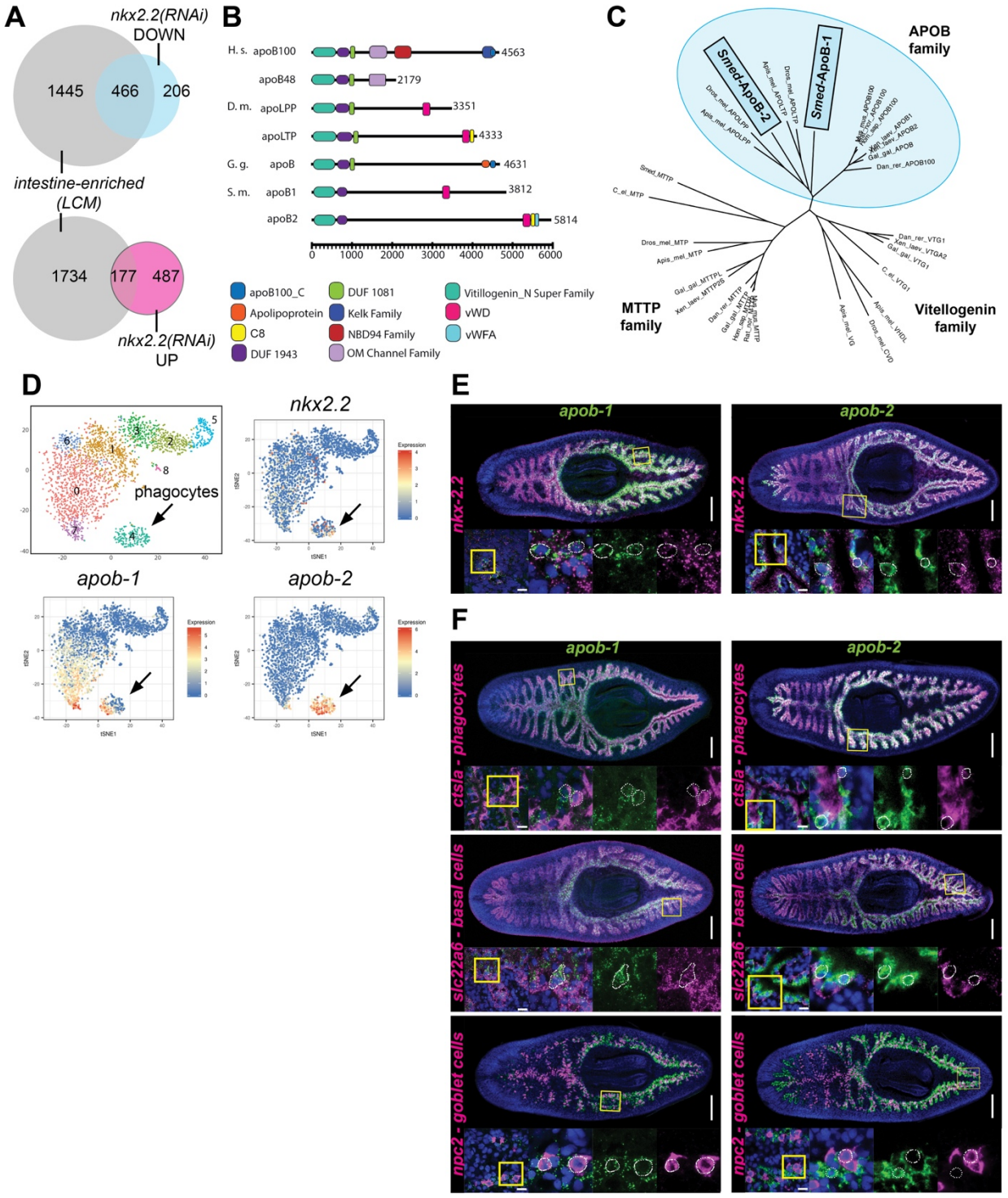

1128

Figure S1.

1129

1130 **Figure S1. *apob-1* and *apob-2* encode intestine-enriched ApoB orthologs. (A)** Overlap of
1131 downregulated (top) and upregulated (bottom) transcripts in *nkx2.2(RNAi)* animals with
1132 intestine-enriched transcripts. 466/672 downregulated and 177/664 upregulated genes were
1133 present in intestine-enriched data set (Forsthoefel et al., 2020); total numbers of dysregulated
1134 transcripts in *nkx2.2(RNAi)* samples were slightly lower than Table S1, because some did not
1135 have detectable expression in the intestine data set. **(B)** Conserved domains in human (H.s.), fly
1136 (D.m.), chicken (G.g.), and planarian (S.m.) ApoB proteins. **(C)** Phylogenetic relationship of
1137 planarian (*Smed*) ApoB-1 and ApoB-2 N-terminal Vitellogenin domains those of closely related
1138 ApoB and Vitellogenin-domain-containing proteins in human (*Hom_sap*), mouse (*Mus_mus*),
1139 chicken (*Mus_mus*), fly (*Dros_mel*), honeybee (*Apis_mel*), frog (*Xen_laev*), and *C. elegans*
1140 (*C_el*). **(D)** t-SNE plots from single cell transcriptomes (Fincher et al., 2018) showing expression
1141 of *nkx2.2, apob-1,* and *apob-2* in the intestinal lineage. All transcripts were enriched in progeny
1142 (subclusters 0/7) and mature phagocytes (arrow); *nkx2.2* was also present in
1143 neoblasts/transition state (subcluster 1). **(E)** Double FISH showing co-expression of *apob-1,*
1144 *apob-2,* and *nkx2.2* mRNA. **(F)** Double FISH showing expression of *apob-1, apob-2* in
1145 phagocytes and basal cells (*apob-1 only*), but not goblet cells. Scale bars: 200 µm **(D-E)**; 10 µm
1146 **(D-E** insets, bottom left**).**
1147

1148

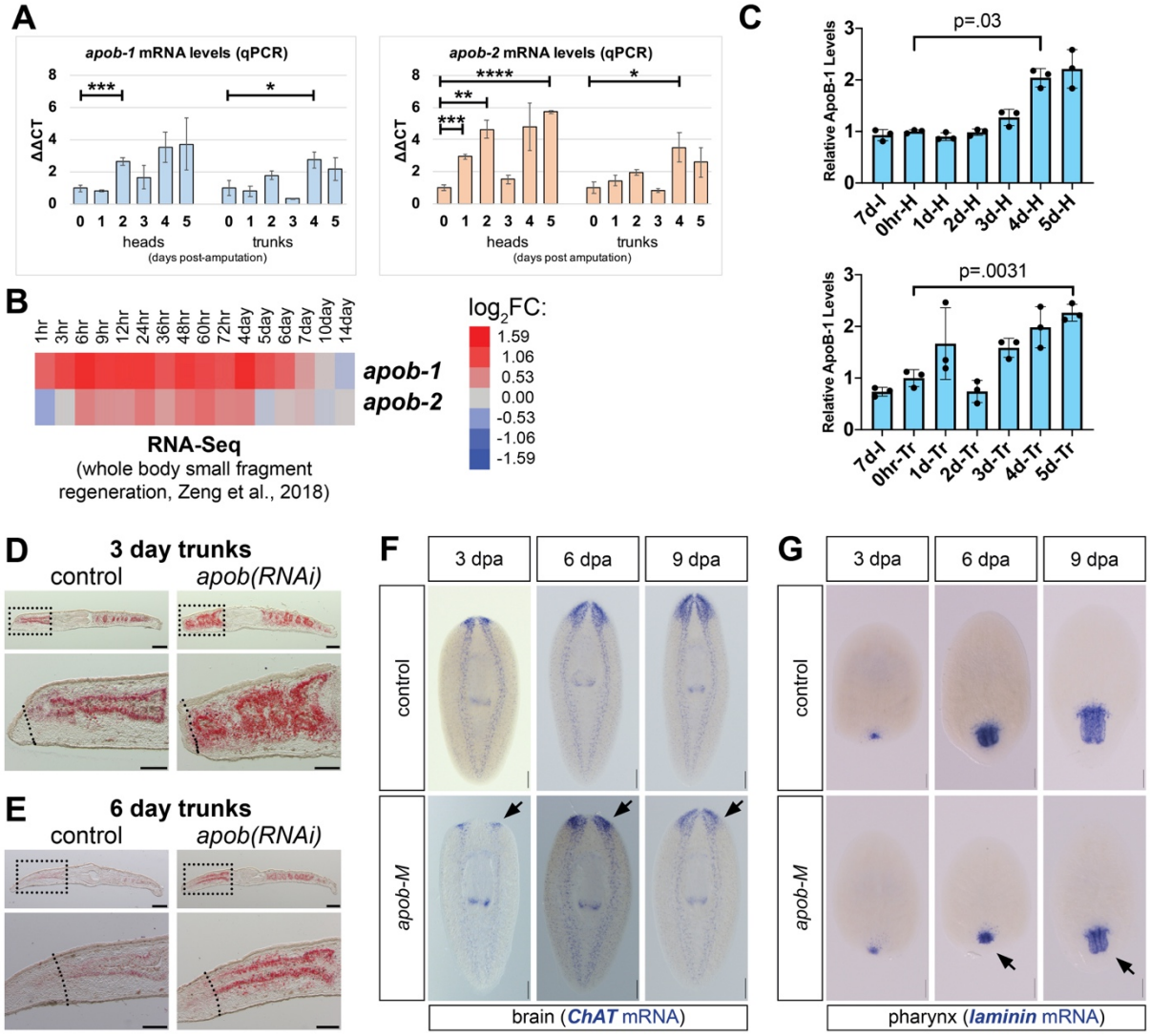

1149

1150 **Figure S2.**

1151 **Figure S2. Further characterization of *apob* expression and RNAi phenotypes. (A)** *apob-1*
1152 and *apob-2* mRNA levels are upregulated in head and trunk regenerates (qRT-PCR). **(B)** *apob-*
1153 *1* and *apob-2* mRNA levels are upregulated in whole fragment RNA-Seq data (Zeng et al.,
1154 2018). **(C)** ApoB-1 protein is upregulated during regeneration (3-5 dpa) in head and trunk
1155 fragments. **(D-E)** Neutral lipids accumulate in *apob*(RNAi) ("mild") regenerates. Dashed line
1156 indicates approximate plane of amputation. Anterior is left. **(F-G)** Brain and pharynx
1157 regeneration are delayed, but not blocked, by *apob* RNAi. Arrows indicate smaller organs in
1158 *apob-M* animals relative to controls (representative images). Significance testing (qPCR):
1159 Student's t-test (two-tailed, heteroschedastic) on pairwise comparisons to 0 day time points.
1160 Significance testing (Wes): one-way ANOVA (multiple comparisons) with Dunnet's T3 test. DAPI
1161 (blue) in **(D-G)**. Error bars = mean +/- S.D. Error bars = mean +/- S.D. Scale bars: 200 μm **(D-E,**
1162 upper panels**)**; 100 μm **(D-E,** lower panels**)**; 100 μm **(F-G)**.
1163

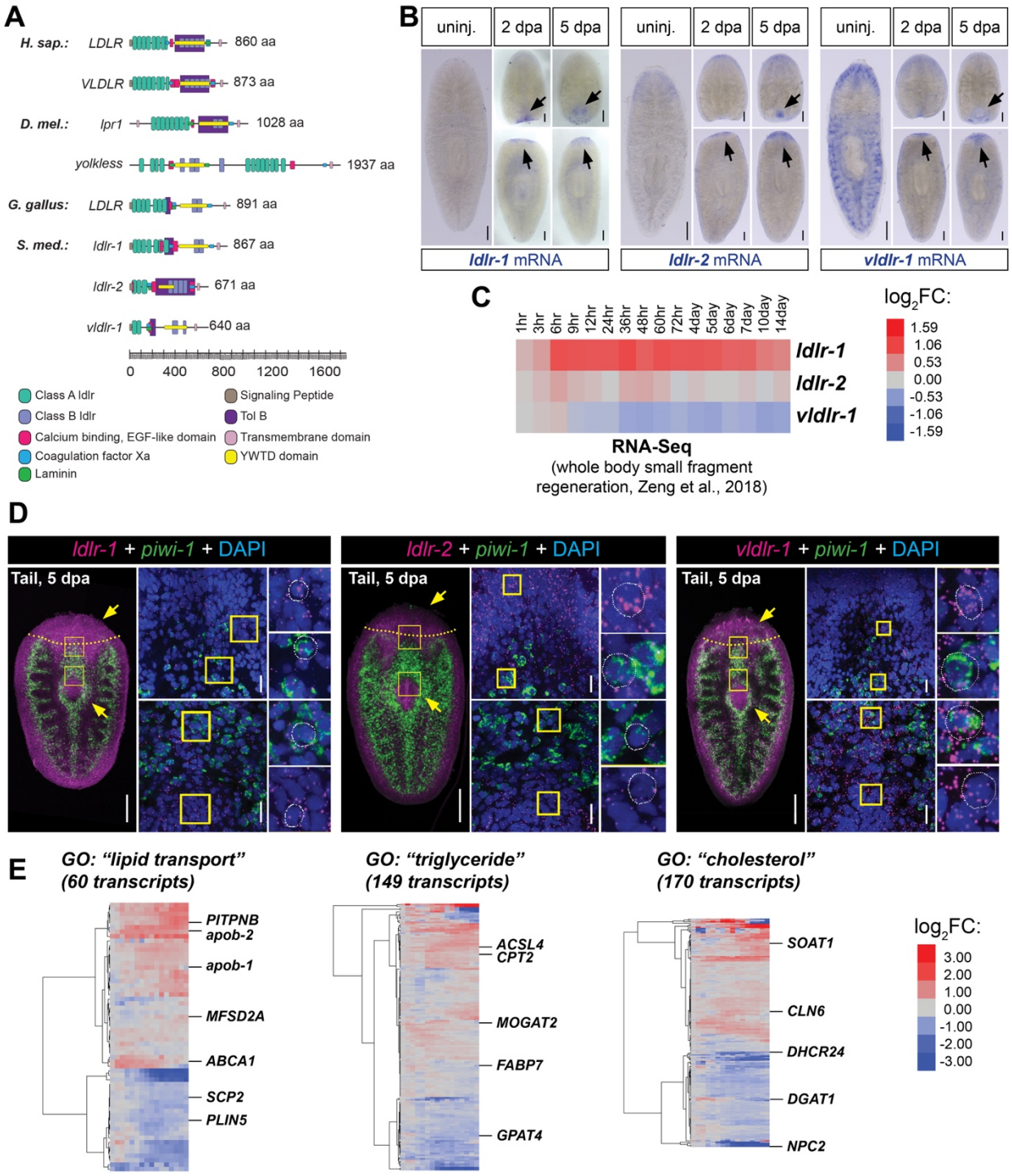
A
H. sap.: LDLR 860 aa
VLDLR 873 aa
D. mel.: lpr1 1028 aa
yolkless 1937 aa
G. gallus: LDLR 891 aa
S. med.: ldlr-1 867 aa
ldlr-2 671 aa
vldlr-1 640 aa
0 400 800 1200 1600
Class A ldlr
Class B ldlr
Calcium binding, EGF-like domain
Coagulation factor Xa
Laminin
Signaling Peptide
Tol B
Transmembrane domain
YWTD domain
B
uninj. 2 dpa 5 dpa
ldlr-1 mRNA
ldlr-2 mRNA
vldlr-1 mRNA
C
1hr 3hr 6hr 9hr 12hr 24hr 36hr 48hr 60hr 72hr 4day 5day 6day 7day 10day 14day
ldlr-1
ldlr-2
vldlr-1
log2FC:
1.59
1.06
0.53
0.00
-0.53
-1.06
-1.59
RNA-Seq
(whole body small fragment regeneration, Zeng et al., 2018)
D
ldlr-1 + piwi-1 + DAPI
ldlr-2 + piwi-1 + DAPI
vldlr-1 + piwi-1 + DAPI
Tail, 5 dpa
E
GO: "lipid transport" (60 transcripts)
PITPNB
apob-2
apob-1
MFSD2A
ABCA1
SCP2
PLIN5
GO: "triglyceride" (149 transcripts)
ACSL4
CPT2
MOGAT2
FABP7
GPAT4
GO: "cholesterol" (170 transcripts)
SOAT1
CLN6
DHCR24
DGAT1
NPC2
log2FC:
3.00
2.00
1.00
0.00
-1.00
-2.00
-3.00

Figure S3.

1167 **Figure S3. Lipoprotein receptors are upregulated during planarian regeneration. (A)**
1168 Schematic showing domains in LDLR and related homologs. **(B)** WISH showing upregulation of
1169 planarian *ldlr* homologs in blastemas at 2 and 5 dpa. **(C)** *ldlr-1* and *ldlr-2* mRNA levels are
1170 upregulated in whole fragment RNA-Seq data (Zeng et al., 2018). **(D)** *ldlr* homologs (magenta,
1171 mRNA FISH) are expressed in *piwi-1*+ neoblasts (green, mRNA FISH) as well as differentiating
1172 (*piwi-1*-negative*)* brain and pharynx (arrows). **(E)** Heat maps showing numerous planarian
1173 transcripts related to lipid metabolism are up- and down-regulated during regeneration in whole
1174 fragment RNA-Seq data (Zeng et al., 2018). Scale bars: 200 μm **(B)**; 200 μm **(D,** left panels**)**; 20
1175 μm **(D,** right panels**)**.
1176

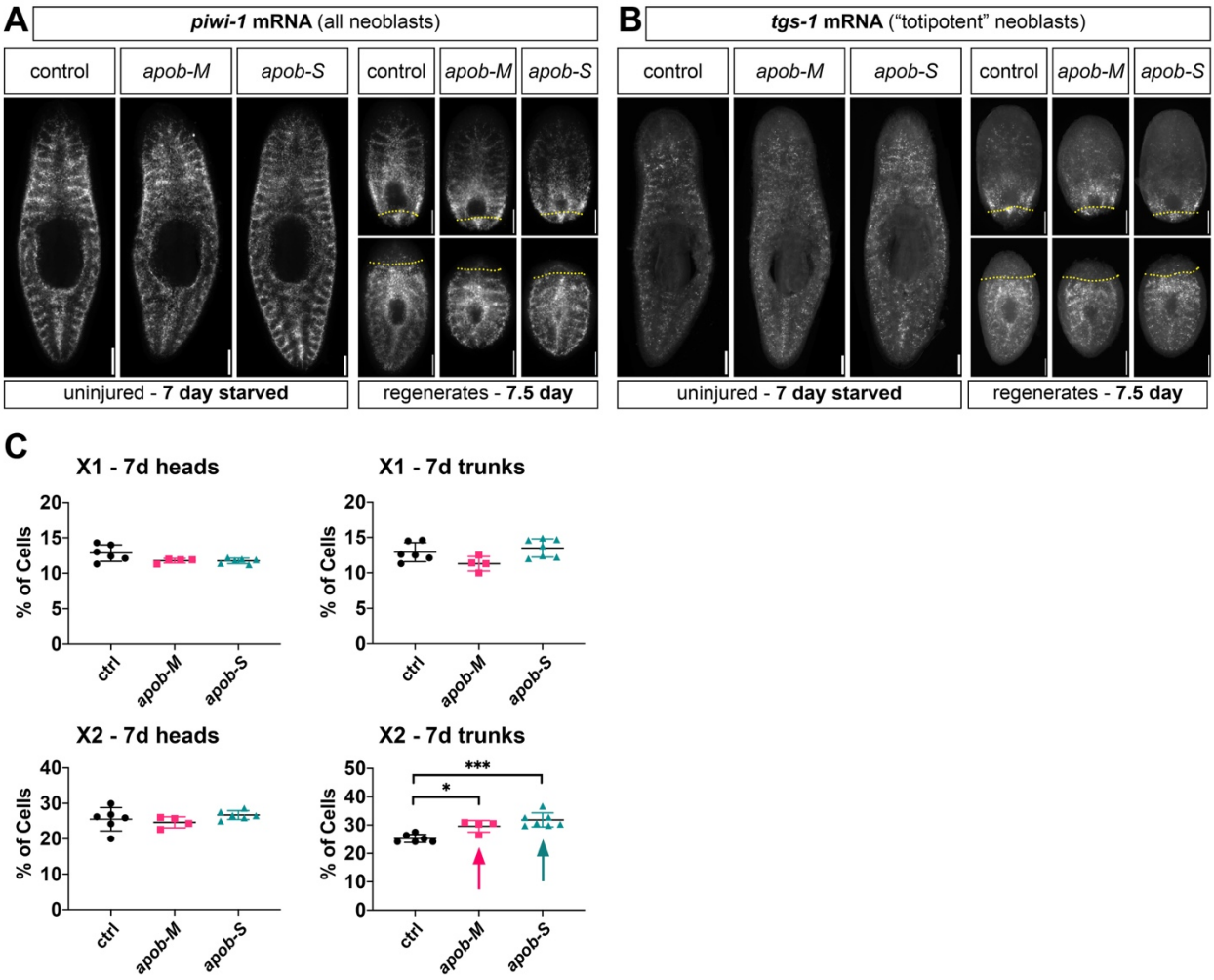

1177

1178

1179 **Figure S4.**

1180 **Figure S4. Further characterization of effects of *apob* inhibition on neoblasts and**
1181 **neoblast progeny. (A-B)** Numbers and body-wide distribution of of *piwi-1+* and *tgs-1+*
1182 ("totipotent") neoblasts are grossly normal in uninjured (left panels) and 7.5 dpa head and tail
1183 regenerates (right panels). Whole-mount FISH, representative samples, epifluorescent images.
1184 Dotted lines, approximate amputation plane. **(C)** Percentage of cells in X1 and X2 in 7 day head
1185 (left) and trunk (right) regenerates. Arrows indicate significant increases in X2. Flow cytometry
1186 significance testing: one-way ANOVA and Tukey's multiple comparisons test. Error bars = mean
1187 +/- S.D. Scale bars: 200 μm **(A-B)**.
1188

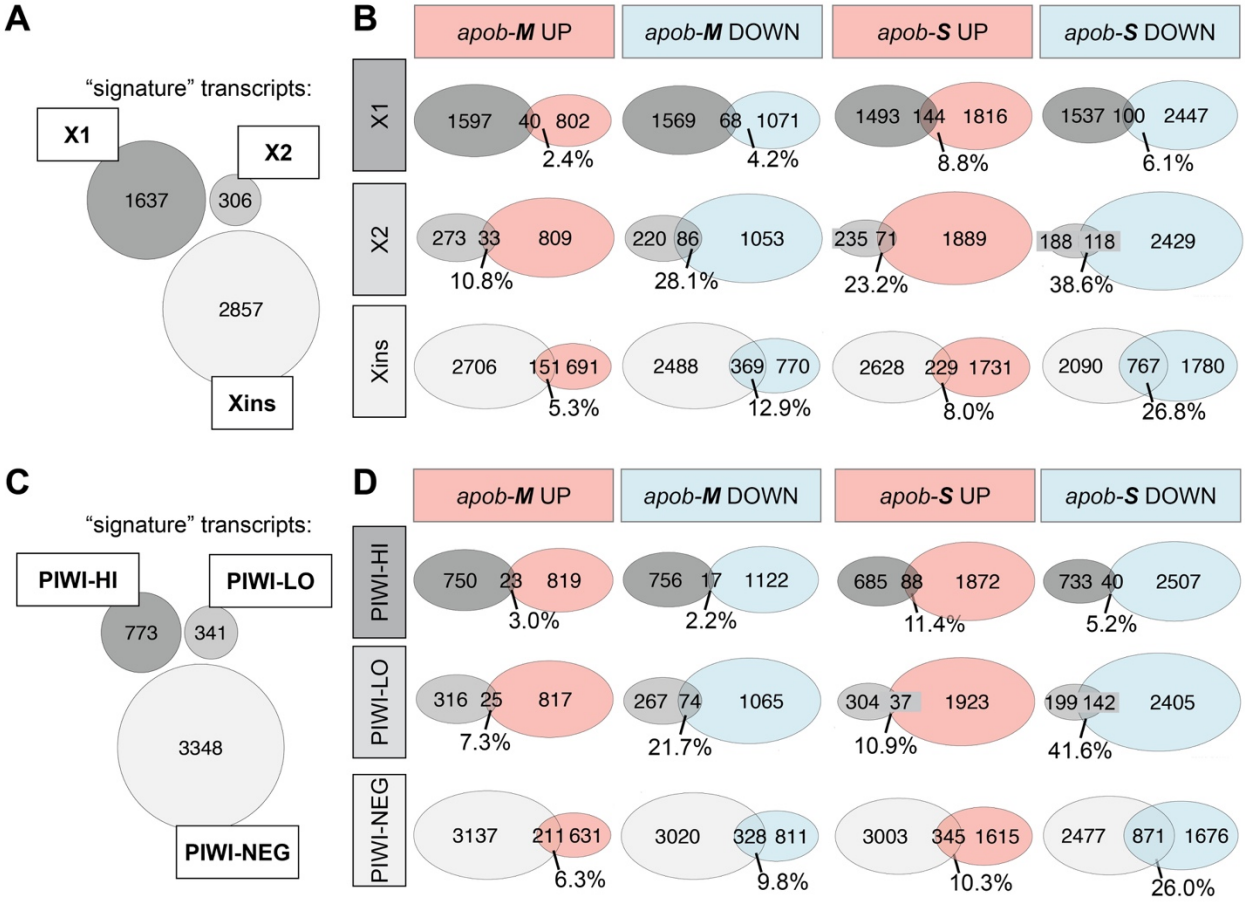

1189

1190

1191 **Figure S5.**

1192 **Figure S5. *apob* RNAi preferentially dysregulates transcripts in differentiating neoblast**
1193 **progeny and mature post-mitotic cells. (A)** Venn diagram showing no overlap between X1,
1194 X2, and Xins "signature" transcripts (defined as having logFC>1 (FDR<.05) vs. transcripts in
1195 both other fractions). **(B)** Venn diagrams showing overlap between X1, X2, and Xins signature
1196 transcripts and transcripts up or down in *apob-M* and *apob-S*. Percentages of X1/X2/Xins
1197 dysregulated are indicated. **(C)** Venn diagram showing no overlap between PIWI-HI, PIWI-LO,
1198 and PIWI-NEG signature transcripts (defined as having logFC>1 (FDR<.05) vs. transcripts in
1199 both other fractions). **(D)** Venn diagrams showing overlap between PIWI-HI, PIWI-LO, and
1200 PIWI-NEG signature transcripts and transcripts up or down in *apob-M* and *apob-S*. Percentages
1201 of PIWI-HI/PIWI-LO/PIWI-NEG dysregulated are indicated.
1202

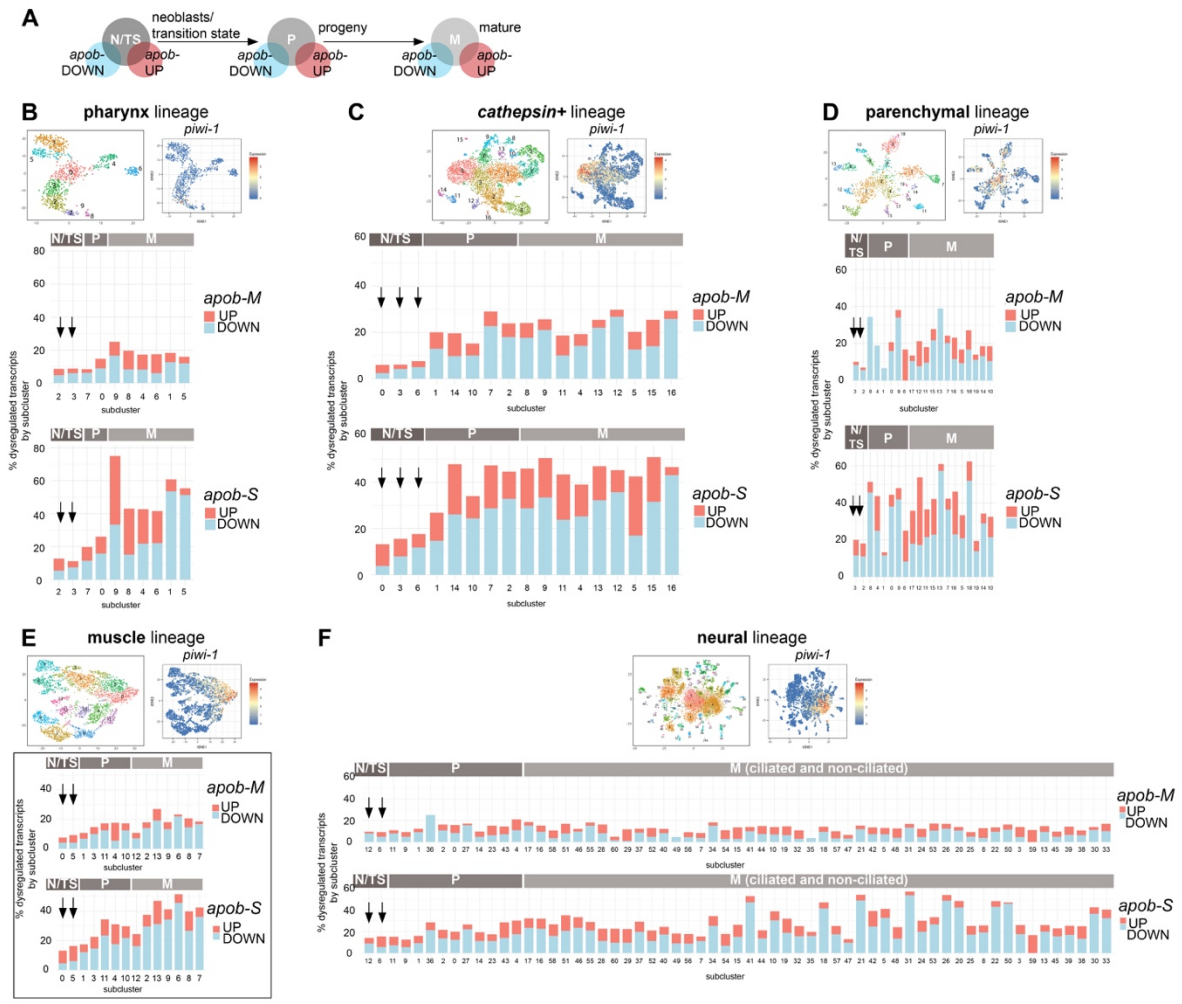
A
neoblasts/
transition state
progeny
mature
N/TS
P
M
apob-
DOWN
apob-
UP
B pharynx lineage
C cathepsin+ lineage
D parenchymal lineage
E muscle lineage
F neural lineage
piwi-1
apob-M
apob-S
UP
DOWN
% dysregulated transcripts
by subcluster
subcluster
M (ciliated and non-ciliated)

Figure S6.

1214 **Figure S6. Additional examples of dysregulation of transcripts in differentiating neoblast**
1215 **progeny and mature post-mitotic cells by *apob* RNAi. (A)** Venn diagram depicting generic
1216 scheme used to identify overlap of transcripts enriched in specific subclusters in Fincher et al.,
1217 2018 that are dysregulated in *apob(RNAi)* planarians. **(B-F)** *apob* knockdown dysregulates
1218 greater proportions transcripts in progeny ("P") and mature ("M") post-mitotic subclusters (based
1219 on *piwi-1* mRNA levels, see Methods) in multiple cell type lineages. Arrows indicate less-
1220 affected transcripts in neoblast/transition state ("N/TS") subclusters. t-SNE plots
1221 (digiworm.wi.mit.edu) indicate subclusters and *piwi-1* mRNA expression in progenitors/early
1222 progeny.
1223

1224 ## Supplemental Tables

1225

1226 **Table S1. Up- and downregulated transcripts in *nkx2.2(RNAi)* planarians.**

1227

1228 **Table S2. Gene Ontology Biological Process terms enriched for transcripts up- and**

1229 **downregulated by *nkx2.2* RNAi.**

1230

1231 **Table S3. Transcripts annotated with lipid-related Gene Ontology terms in the planarian**

1232 **transcriptome.**

1233

1234 **Table S4. Up- and downregulated transcripts in *apob-1;apob-2(RNAi)* "mild" and "severe"**

1235 **planarians.**

1236

1237 **Table S5. Gene Ontology Biological Process terms enriched for transcripts up- and**

1238 **downregulated by *apob* RNAi.**